Materials Advances

ROYAL SOCIETY OF CHEMISTRY

REVIEW

View Article Online
View Journal | View Issue

Cite this: *Mater. Adv.*, 2021, 2, 3519

2D nanosheet enabled thin film nanocomposite membranes for freshwater production – a review†

Deepak Surendhra Mallya, *[a] Ludovic F. Dumée, *[bcd] Shobha Muthukumaran, [e] Weiwei Lei [f] and Kanagaratnam Baskaran [a]

Received 25th March 2021,
Accepted 12th May 2021

DOI: 10.1039/d1ma00256b

rsc.li/materials-advances

Thin film composite (TFC) membranes are primarily used for commercial desalination and water purification applications by both reverse osmosis (RO) and nanofiltration (NF). The incorporation of 2D nanosheets across TFC membranes during interfacial polymerization generates a novel class of separation materials with higher permeability and selectivity, as well as greater chemical and thermal stabilities, supporting antifouling behaviours. Here, the potential of 2D nanosheet-based TFN to engineer materials of enhanced separation properties are critically discussed, in light of defect engineering approaches, types of unique properties of various nanosheets and Case studies on 2D nanosheet-based TFN membranes are critically compared, and properties-to-performance relationships are established to reveal trends and provide insights on the future of the field. The impact of the 2D nanosheets on the surface properties and interactions with solutes in water are extensively discussed. Challenges related to the TFN fabrication processes and leaching of nanosheets over time, which diminishes the scalability and long-term separation performance are also discussed. A vision for advanced and scalable manufacturing synthesis of nanosheets assemblies across or within TFN membranes is also evaluated alongside potential strategies to support the next generation of 2D-enabled separation membranes.

[a] *School of Engineering, Deakin University, Waurn Ponds 3216, Australia. E-mail: dmallya@deakin.edu.au, basbaskaran@deakin.edu.au*
[b] *Khalifa University, Department of Chemical Engineering, Abu Dhabi, United Arab Emirates. E-mail: ludovic.dumee@ku.ac.ae; Tel: +971563842672*
[c] *Research and Innovation Center on CO2 and Hydrogen, Khalifa University, Abu Dhabi, United Arab Emirates*
[d] *Center for Membrane and Advanced Water Technology, Khalifa University, Abu Dhabi, United Arab Emirates*
[e] *College of Engineering and Science, Victoria University, Melbourne 14428, Australia. E-mail: Shobha.Muthukumaran@vu.edu.au*
[f] *Institute of Frontier Materials, Deakin University, Geelong, Victoria 3220, Australia. E-mail: weiwei.lei@deakin.edu.au*
† Electronic supplementary information (ESI) available. See DOI: 10.1039/d1ma00256b

Deepak Surendhra Mallya

Deepak Surendhra Mallya completed his bachelor's degree in Chemical Engineering at SASTRA Deemed to be University, in 2018. He is currently a Doctoral candidate in the School of Engineering at Deakin University. His research focus includes 2D material synthesis and application in next-generation membranes for desalination and removal of emerging contaminants.

Ludovic F. Dumée

A/Prof. Ludo DUMEE is a materials engineer interested in the development and application of advanced separation materials, primarily focused on membranes and catalysts. His research interests lay in the understanding of nanoscale interactions between contaminants and surfaces as well as the design of reactive and stimuli-responsive materials in the water, gas and healthcare applications. He currently leads the Advanced Separation team at Khalifa University focused on engineering combinatorial materials including carbon allotropes and ceramics nano-coatings to control the texture and reactivity of separation materials at the nanoscale. He works on the remediation of pressitent contaminants including PFAS, microplastics and on the selective recovery of resources from complex solutions.

1. Introduction

Reverse osmosis (RO) and nanofiltration (NF) membrane technologies are currently the most valuable and applied commercial technology to desalinate water. State-of-the-art RO and NF membranes are based on thin film composite (TFC) structures, which usually consist of a thin selective poly(amide) (PA) layer deposited over a range of porous supporting layers. The PA layer is formed by Interfacial Polymerization (IP) at the interface between an aqueous and an organic phase containing otherwise insoluble self-reactive monomers.[1] The PA layer governs the physiochemical properties and separation performance of TFC membranes and is optimized by controlling the free volume across this layer to enable specific salt rejection but allow water transport upon overcoming the osmotic pressure of a solution. The incorporation of specific functional monomers and additives and the control of the IP reaction parameters, such as the monomer concentration, or post-treatment conditions, have enabled the development of a range of versatile membrane materials.[2] Conventional TFC membranes suffer from disadvantages like a trade-off between permeability and salt rejection, inevitable fouling tendencies and relative instability towards chlorine which is used for chemical cleaning.[3] Hence, membranologists are constantly trying to develop innovative bridges to tackle these shortcomings and fabricate next generation membranes which offer superior performance at lower operating costs.[4]

The use of nanomaterials as additives during the IP reaction yields a new class of membranes, referred to as Thin Film Nanocomposite (TFN) membranes. Since the introduction of the TFN concept in 2007, various types of nanomaterials ranging from carbon allotropes, metal and oxide nanoparticles, cellulose nanocrystals, and both inorganic and organic crystalline frameworks have been incorporated into membrane materials, offering different functionalities as well as surface properties.[5–10] The incorporation of nanomaterials has been found to alter the PA layer cross-linking levels and thus free volume distribution across the layer.[11] Control over the IP chemistry has also enabled the fine-tuning of morphological features, such as thickness, pore size and roughness, and surface properties, including the surface charge and hydrophilicity, resulting in materials with higher permeability and selectivity, as well as stronger antifouling properties.[9,11,12] Depending on the types of additives, TFN membranes have also showed enhanced anti-microbial, thermal, mechanical and chemical stability.[5,13]

Two-dimensional (2D) nanosheets have been recently employed in the fabrication of TFN membranes. The unique properties of 2D nanosheets, including their atomic thickness, extreme surface charge and plasmonic characteristics, and the emergence of scalable production routes have paved the way for a new class of 2D-enabled TFN membranes, predicted to offer enhanced

Shobha Muthukumaran

Shobha Muthukumaran is an Associate Professor in the College of Engineering and Science at the Victoria University, Melbourne, Australia. Shobha completed her PhD at Melbourne University, Australia. Before her PhD, Shobha worked in the environmental engineering industries in different capacities for over nine years. She has more than fourteen years of teaching experience in Higher Education in the fields of water and environmental engineering. Shobha has also conducted extensive research in water and wastewater management for more than twenty years. She has published more than 100 journal and conference publications, 3 book chapters and several technical reports.

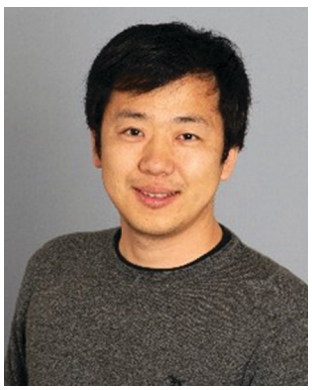

Weiwei Lei

A/Prof. Weiwei Lei received his PhD degree from the Jilin University in China. He then joined Max-Planck-Institute of Colloids and Interfaces, Germany, as Research Fellow. He was awarded Alfred Deakin Postdoctoral Research Fellowship in 2011 and Australian Research Council Discovery Early Career Researcher Award (DECRA) in 2014. He is currently leading a research group of Plasma Technique and Functionalization Materials in Institute for Frontier Materials (IFM). He has published more than 140 peer reviewed papers in high impact journals including Nature Communications, Joule, Journal of the American Chemical Society, and Advanced Materials.

Kanagaratnam Baskaran

Professor Baskaran has more than 35 years of professional experience in Civil and Environmental Engineering. He joined Deakin University as a Lecturer in 1992 and actively involved in the development and delivery of several undergraduate and postgraduate programs in engineering. His areas of research expertise include integrated urban and industrial water management, water recovery and reuse, wastewater treatment technologies, and industrial pollution prevention and control. Prof. Baskaran also has extensive knowledge and understanding for the Australian Water Industry and successfully completed several industry funded research projects over the past 25 years.

performance compared to commercial TFC membranes.[14] Graphene oxide (GO) and its derivatives are among the most promising 2D nanosheet materials, owing to their lower costs of production and tunable surface chemistries.[15] Among other emerging 2D nanosheets showing great promise are boron nitride[9] (BN), molybdenum disulfide[14] (MoS_2), metal carbides[16] (MXenes), graphitic carbon nitride[17] (g-C_3N_4), and covalent organic frameworks[18] (COF). Recent reviews of TFN membranes have primarily focused on bringing together studies on the incorporation of various nano-scale particulate matter for water treatment applications.[19–22] Challenges associated with the fabrication, scale-up and commercialization of some of these materials have been discussed.[23–25] Laminar membranes, assembled solely by stacking 2D nanosheets,[26] exhibit similar performance profiles as TFN membranes, and several reviews on laminar and 2D-enabled mixed matrix membranes have also broadly focused on advanced synthetic pathways and their applications for liquid, gas and ion separation.[25,27] Yet, despite the potential of laminar membranes, TFN membranes appear currently better suited in the short term to serve commercial needs and tackle current separation challenges, since they offer more scalable and cost-effective solutions compared to laminar membranes.[25,28] The composition, structure and selection criteria of nanomaterial based fillers for TFN membranes was briefly discussed along with its application in gas and liquid separation.[29] A recent review paper put together a discussion on different nanosheet embedding strategies and the impact of the processes on the performance of the membranes.[30] However, this manuscript is limited to common mechanisms and function of TFN membranes, and lacks distinctive perspectives on sheet/polymer interactions as well as a detailed summary of recent developments of the 2D nanosheets on the physicochemical properties of the membrane. The challenges associated with TFN membrane fabrication and potential future perspectives are overlooked to date, while critical analysis on prospect of the field is needed.

The focus of this critical essay is to review and compare recent advances in 2D nanosheets-enabled TFN membranes for both RO and NF developed for water treatment applications. A summary of 2D-enabled TFN membranes involving various additives is discussed in terms of surface properties and performance, with emphasis on the impact of 2D nanosheets on the PA layer and membrane performance. The performance of these membranes is then compared with that of commercial benchmarked membranes to establish a roadmap for future 2D-enabled TFN membranes whose applications go beyond those of conventional TFC membranes. The fantastic properties of nanocomposite membranes can open the gateway to catalytic, self-cleaning and reactive membranes for water treatment,[31,32] gas separation,[33] environmental remediation of persistent chemicals and pharmaceutical,[8,34] and medical applications.[34,35]

2. Interfacially polymerized 2D-enabled TFN membranes

The global market of NF and RO membranes is dominated by the interfacially polymerized PA TFC structure due to its superior performance and durability, easy fabrication strategy and industrial scale-up options.[23,36,37] The top selective PA layer is 10–200 nm thick, with porous polymer support—usually poly(ethersulfone) (PES) or poly(sulfone) (PSf) usually 30–50 μm thick.[2] Polycondensation reactions of polyamine monomers and polyacyl halides at the interface lead to formation of the PA layer.[1] The most common organic phase monomer used is trimesoylchloride (TMC), while metaphenylenediamine (MPD) and piperazine (PIP) are used as aqueous phase monomers to fabricate the aromatic PA layer for RO and aliphatic polypiperazine amide (PPA) layer for NF.[22,38] As shown in Fig. 1a, the porous membrane surface is contacted with aqueous and organic phases, subsequently initiating the IP reaction which is self-inhibiting, and leading to the formation of a thin PA layer.[9] The concentration of amine monomer is the rate limiting factor during IP. The optimum concentration of MPD and PIP are maintained at 2 wt% and between 1–2 wt% for RO and NF membranes, respectively. The organic phase monomer TMC, is usually in the concentration range of 0.1–0.3 wt%. A high ratio of amine-to-acid chloride is maintained to facilitate complete polymerization, formation of amide bonds and enhance the crosslinking degree of the PA network.[39] The IP reaction is terminated by heat curing to evaporate excess solvent and initiate further crosslinking of the PA layer.[22,40] Heat curing strategy is debatable as it leads to deterioration of membrane structure and performance given the high temperature and long curing time. Hot air oven, solvent-assisted and microwave heating are a few methods implemented.[40,41]

There are three main pathways to generate TFN from 2D nanosheets. First, TFN membranes may be fabricated by incorporating the nanosheets into either the aqueous or the organic phase

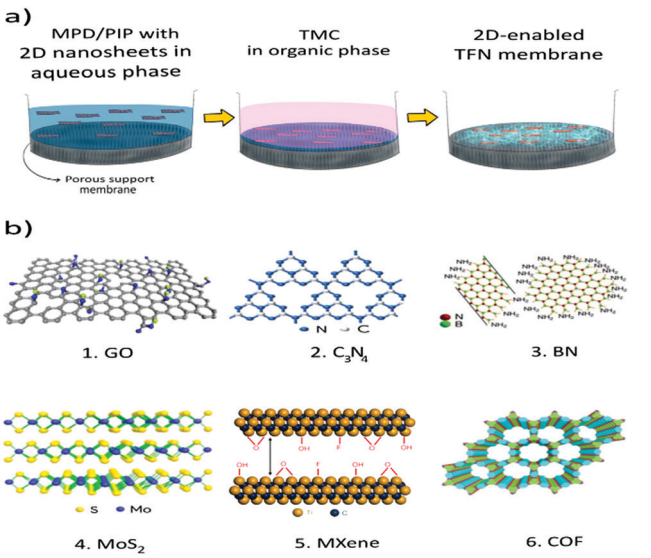

Fig. 1 (a) Fabrication of 2D-enabled TFN membranes *via* IP reaction; (b) illustrations of various 2D materials for TFN membranes. (1) GO, Adapted with permission.[143] Copyright 2015 Springer Nature. (2) g-C_3N_4, Adapted with permission.[17] Copyright 2020 Elsevier. (3) BN, Adapted with permission.[74] Copyright 2015 Springer Nature, (4) MoS_2, Adapted with permission.[78] Copyright 2018 Elsevier. (5) MXene (Titanium based structure), Adapted with permission.[144] Copyright 2018 Springer Nature. (6) COF (triphenyle and pyrene-based structure). Adapted with permission.[145] Copyright 2008 Wiley-VCH.

during the IP reaction. Second, the nanosheets may be incorporated into the substrate material or as an interlayer between the substrate and the PA layer to support the formation.[42,43] Last, 2D nanosheets may be applied onto the surface of the membranes to decorate the PA layer in a controlled manner.[44,45] The conventional IP reaction involves removal of the aqueous phase, utilizing rubber roller or airgun or air knife. Emerging innovations open up methods such as vacuum filtration, spin coating and electrospraying-assisted IP reaction techniques which facilitate the contact of the aqueous phase on the support membrane. This review paper brings together and systematically analyses TFN membranes incorporated with 2D nanosheets during the IP reaction into aqueous or organic phases. The following sections summarizes the recent studies involving 2D-enabled TFN membranes focussing on nanomaterials including GO, g-C_3N_4, BN, MoS_2, MXenes and COF due to its relevance and emerging trends in the research field. The schematic illustration of different 2D structures is shown in Fig. 1b.

2.1. GO enriched TFN membranes

Graphene oxide (GO) is a carbon-based nanomaterial that has received tremendous research attention for its role as nanofiller in TFN membrane fabrication. Its desirable properties include atomic thickness, smoothness, and abundant availability of oxygen functional groups on its surface, facilitating higher rate of water transport through its nanochannels.[21,46,47] The incorporation of GO across the PA layers of TFC membranes produces membranes with improved hydrophilicity and enhanced performance.[5,48,49] TFN RO membranes embedded with GO in the PA layer exhibited high anti-biofouling property and chlorine resistance, combined with high water permeation and maintained high salt rejection (Table S1, ESI,† entry 1).[49] GO nanosheets were fabricated *via* chemical exfoliation and fractionated using 5 μm trach-etch membrane to ensure precise control over the size of the nanosheets. The fractionated GO nanosheets were dispersed in aqueous solution containing MPD and employed in the IP reaction. At an optimum concentration of 0.0038 wt% of GO nanosheets, the water permeability and anti-biofouling properties of the TFN membrane improved by 80% and 98%, respectively. The salt rejection for NaCl was enhanced from 99.28% to 99.40%. The modified membrane maintained salt rejection >99% after direct chlorination for 24 h at 2000 ppm of NaOCl exposure. The presence of oxygen-containing functional groups on the surface of GO nanosheets improved the hydrophilicity of the membranes through hydrogen bonding with water molecules. Electron microscope images of TFN membranes incorporated with non-fractionated GO displayed abnormal surface morphology. Use of GO nanosheets of size >10 μm was observed to impact the MPD diffusion during IP reaction and facilitate visible aggregation in the PA layer.

TFN RO membrane fabricated by incorporating 0.01 wt% GO in aqueous phase exhibited enhanced water permeance, mechanical stability, antifouling performance and chlorine resistance (Table S1, ESI,† entry 2).[13] Water permeance improved by 39%, accompanied by salt rejection of 98% for NaCl. However, on further increasing the GO content, the permeance and salt rejection properties deteriorated due to aggregation and formation of localized defects. When the operating pressure was beyond 25 bar, the control TFC membrane exhibited sharp decline in salt rejection to <80% while the TFN membrane maintained a stable salt rejection >95%. The decline in salt rejection was attributed to the deformation of the membrane under mechanical stress. GO nanosheets with intercalation behaviour led to reinforcement of the skin layer and improved the mechanical stability of the resultant membrane. The improved hydrophilicity and negative charge on addition of GO resulted in higher antifouling performance. Compared to the control TFC membrane with water flux recovery at 50%, the TFN membrane showcased 85% recovery. Chlorine exposure experiments revealed that the TFN membrane exhibited stable performance when compared to the control membrane. The improved chlorine resistance was attributed to the formation of hydrogen bonds between amide groups of the PA matrix and GO nanosheets, offering protection against chlorine. A study reported that TFN RO membrane incorporated with GO offered higher water permeance, organic removal and antifouling performance.[50] At an optimum loading of 0.004 wt% of GO in the aqueous phase, permeance increased by 27%. Fouling experiments after 5 h showed that membranes incorporated with GO had moderate reduction of less than 10% in flux when compared to control membranes at 14% reduction. In addition, organic removal doubled in the case of the TFN membrane. The improved membrane surface hydrophilicity and negative charge enhanced antifouling and organic removal properties.

Application of GO for TFN NF membranes has also been explored.[48,51] Incorporating GO at an optimum loading of 0.2 wt% resulted in a twelve-fold increase in water permeance, with negligible 1% decline in salt rejection, accompanied by high antifouling performance (Table S2, ESI,† entry 1).[48] It was also observed that in addition to improved hydrophilicity, negative charge and enhanced surface morphology, formation of nano voids in PA due to addition of GO enhanced the performance of the membranes. The membranes exhibited higher normalized flux at 95% and 95% during fouling experiments with bovine serum albumin (BSA) and humic acid (HA) respectively, when compared to the control membrane with values 68% and 44%. However, the permeance reported was very low at 1.48 L m^{-2} h^{-1} bar^{-1}, which is lower than that of commercial membranes.

In the above-mentioned studies, GO nanosheets were incorporated into the aqueous monomer solution. The compatibility of GO with organic solvents provides an alternative route for incorporation in the organic phase during IP reaction. GO nanosheets with a layered structure and an interlayer spacing of around 0.83 nm were dispersed in the organic solution containing TMC in n-hexane (Table S1, ESI,† entry 4).[52] At an optimum GO concentration of 0.015 wt%, the water permeance of the TFN RO membrane increased from 1.88 to 2.87 L m^{-2} h^{-1} bar^{-1}, while the rejection of NaCl and Na_2SO_4 slightly diminished from 95.7% to 93.8% and from 98.1% to 97.3%, respectively. The GO-incorporated TFN membrane also exhibited very good long-term operation stability. At the termination of a 72 h filtration experiment, the membrane exhibited a very stable water flux and salt rejection. Nanochannels formed due to the interlayer spacing in the GO nanosheets apparently provided shorter paths

with lower resistance for water permeation, enhancing the water permeance.

GO-Incorporated TFN membranes have displayed the ability to bridge the trade-off between permeance and selectivity, while exhibiting enhanced antifouling performance. However, the optimum loading might show variations when TFN membranes are designed for improved permeance or fouling resistance. The effect of incorporation of GO nanosheets into the PA layer on permeance and fouling resistance has been extensively studied (Table S1, ESI,† entry 5).[46] GO was dispersed in the organic phase at three different concentrations at 0.0053 (TFN-Low), 0.0107 (TFN-Med) and 0.0160 (TFN-High) wt%. Increasing the GO content resulted in improving the antifouling and anti-microbial properties of TFN membranes. At low concentration of GO, the TFN membrane showed an increase in permeance by 35.29%. However, with increase in GO content the permeance decreased. The performance of the TFN membrane in terms of rejection of NaCl was stable and similar to that of the control membrane at 96%. It was also concluded that the preparation method of the GO is highly influential in imparting specific properties to the TFN membrane. Compared to modified Hummers' GO, Staudenmaier GO had a lower impact on membrane permeance and selectivity, while enhancing the anti-fouling and antibacterial properties tremendously. Such difference in performance could be attributed to its varied chemical compositions.[53]

It has also been observed that the effects of incorporating GO in terms of membrane permeation performance appeared to be constrained, though GO is seen as a better candidate to mitigate fouling and as antibacterial agent.[46] This facilitated the fabrication of TFN RO membranes incorporated with *p*-aminophenol-modified GO (mGO) into the PA layer (Table S1, ESI,† entry 6).[54] The membrane incorporated with mGO at 0.003 wt% showed enhanced water permeance by 24.6% compared to the control TFC membrane, while maintaining a high rejection of 99.7% for NaCl. The water permeance and salt rejection exhibited initial increase and then declined as the loading of mGO was increased. Membranes incorporated with 0.005 wt% of mGO outperformed both membranes incorporated with GO and control TFC membranes in terms of bacterial killing ratios, which were 96.78% and 96.26% against *E. coli* and *S. Aureus* respectively. This was ascribed to the following reasons: the attached phenolic groups on the mGO structure improved the bactericidal property of the membranes; the hydroxyl groups on the aminophenol group improved anti-bacterial property through oxidative stress reaction in bacteria.[55] In addition, the electron receptor property of mGO helped attract bacteria, and the sharp edges of the mGO structure facilitated their destruction and death.[56] However, in terms of water permeance and salt rejection, the performance of mGO-incorporated membranes was lower than that of GO-incorporated membranes, and this was attributed to its lower hydrophilicity.

The presence of oxygenated functional groups on the surface of GO nanosheets provides potential active sites for attaching various nanomaterials and functional groups to the surface, aiding evolution of nanohybrid materials based on GO, which have a wide range of applications.[57] GO nanosheets with different metal and metal oxides including Ag,[58,59] Cu,[60] TiO_2[61] and ZnO[62] have been synthesized and successfully incorporated into the PA layer of TFC membrane, which exhibited excellent separation performance with antifouling and anti-bacterial properties. In a recent study, Ag-GO nanosheets were incorporated into the PA layer to fabricate biofouling-resistant TFN membrane (Table S1, ESI,† entry 7).[58] Incorporation of 0.008 wt% of Ag-GO nanosheets showed high water flux recovery ratio of 89% and low irreversible fouling at 10% during fouling/cleaning experimentation with BSA solution. It was also observed that the TFN membrane reduced the viable *E. coli* cells by 86% during biofouling studies with bacterial suspensions, with negligible bacterial adhesion on the membrane surface. However, slight reduction in water permeance and salt rejection was observed for Ag-GO TFN membrane when compared to the control membrane. Formation of polyester chains due to incorporation of Ag-GO nanosheets significantly affected the PA layer leading to compromised permeance and salt rejection performance.

GO modified with sulfonic acid was used to prepare TFN NF membrane incorporated with sulfonated graphene oxide (SGO), (Table S2, ESI,† entry 2).[51] The addition of sulfonic groups effectively reduced oxygen functional groups and resulted in partial restacking of nanosheets. Incorporation of 0.3 wt% of SGO exhibited enhancement in water permeance by 87.3% over the control TFC membrane and maintained salt rejection greater than 96.45% for Na_2SO_4. Despite the increased water permeability, the salt rejections were similar to that of the control TFC membrane due to the increased cross-linking and lower MWCO of the SGO-incorporated membrane. Long-term antifouling tests revealed that the SGO-incorporated membrane had good fouling resistance to hydrophilic fraction of NOM, when compared to the pristine TFC membrane, but during filtration studies with HA which is the hydrophobic fraction of NOM, the membranes fouled severely, and the performance was lower than that of the control TFC membrane. Compared to other commercial or TFN membranes, SGO-incorporated membranes had lower membrane permeance, which restricts their application.

In another study, TFN NF membranes incorporated with triethylene tetramine-modified GO (GO-TETA) membranes exhibited enhanced water permeance and antifouling performance (Table S2, ESI,† entry 3).[63] The membranes incorporated with 0.03 wt% GO-TETA exhibited improved water permeance from 8.3 to 12.2 L m^{-2} h^{-1} bar^{-1}. The improved hydrophilicity of TFN membranes resulted in high water flux recovery at 95% after fouling experiments with BSA. The amine functional groups present in the nanosheets also interacted with TMC molecules during IP reaction, impacting the PA layer. The MWCO of the membranes incorporated with 0.03 wt% GO-TETA decreased approximately by two-fold from 565 Da for the control membrane to 300 Da. However, the salt rejection properties were not comparable to those of commercial membranes. The Na_2SO_4 and NaCl rejection was as low as 65.3% and 32.2% respectively. Despite the lowering of MWCO, the positive charge on the membrane surface and transport of salt ions through the

interlayer spacing and the voids between the polymer and nanosheets contributed to lower salt rejection. While incorporation of GO nanosheets into TFN membranes increased the negative surface charge of the membranes partly due to the negatively charged nanosheets, it was noticed that the presence of functional groups can alter and impart specific charge to the nanosheets.

A study reported fabrication of two novel TFN membranes which incorporated positively charged GO nanosheets functionalized with ethylenediamine (EDA) (Table S2, ESI,† entry 4) and polythylenimine (PEI) (Table S2, ESI,† entry 5) respectively.[64] The amine functional groups were grafted through amide bonds without damaging the GO structure. Incorporation of 60 ppm of GO-EDA or 40 ppm of GO-PEI resulted in increasing the water permeance by 54.4% and 60.9% respectively, with salt rejection maintained at over 98%. The nanosheet incorporation led to formation of thinner, smoother and enhanced hydrophilic PA layer and improved the membrane performance. However, the charge properties of the functionalized GO led to variation in the antifouling performance due to its sensitivity to pH. Among these two amine functionalized GO nanosheets, GO-PEI showed superior performance with high permselectivity, antifouling performance, chlorine resistance and mechanical stability, compared to the control membrane.

Maleic anhydride modified GO (MAH-GO) was introduced into the aqueous phase during IP to generate TFN NF membrane with superior performance.[65] MAH-GO incorporation at 0.006 wt% lead to highly hydrophilic, smoother and negatively charged membrane surface. In addition, loose and thin selective PA layer was formed which resulted in enhancing the water permeance by 76.7% to 8.22 L m^{-2} h^{-1} bar^{-1} while maintaining high salt rejection of 97.6% for Na_2SO_4. The TFN membrane also exhibited high antifouling and chlorine resistance performance. Building up on this work, a double modified strategy was implemented to fabricated TFN NF membranes which incorporated MAH-GO in the selective PA layer and SGO into support membrane resulted in enhancement in surface charge, hydrophilicity and thinner selective layer.[66] Incorporation of SGO at 0.1 wt% in the support layer and 0.002 wt% MAH-GO in the selective PA layer increased the water permeance by 33.4% at 14.3 L m^{-2} h^{-1} bar^{-1} compared to control membrane while maintaining Na_2SO_4 rejection at 98% and simultaneously exhibited better antifouling and chlorine resistance performance.

2.2. g-C_3N_4 incorporated TFN membranes

g-C_3N_4 is an emerging 2D nanomaterial analogous to graphene, possessing exceptional thermal and photocatalytic properties besides chemical stability. Its 2D structure consists of tris-triazine units which are linked through amine groups as depicted in Fig. 1b.[67,68] A pioneering study incorporating g-C_3N_4 nanosheets into the PA layer has confirmed improved hydrophilicity, surface roughness and antifouling performance (Table S2, ESI,† entry 6).[67] The TFN NF membrane incorporated with 0.0025 wt% of g-C_3N_4 nanosheets increased the water permeance from 10.45 to 18.8 L m^{-2} h^{-1} bar^{-1} but showed decline in salt rejection to 84% for Na_2SO_4. Fouling-cleaning experiments revealed that both the normalized flux and FRR of the g-C_3N_4 incorporated membrane was higher than that of the control membrane. The improved performance was attributed to the hydrophilicity imparted by g-C_3N_4. However, salt rejection decreased sharply on increased concentrations of g-C_3N_4, which was mainly attributed to the loosening of the PA structure and formation of defects on incorporation of g-C_3N_4 nanosheets. It was also observed that the nanosheets had poor compatibility with the polymer matrix.

Another study incorporated g-C_3N_4 nanosheets as a hydrophilic modifier for TFN RO membranes (Table S1, ESI,† entry 8).[68] This improved the hydrophilicity of the membrane, resulting in enhanced water flux until the concentration of 0.005 wt%, above which the water flux reduced due to the aggregation effect of the nanosheets. Membranes incorporated with 0.015 wt% g-C_3N_4 nanosheets showed the highest NaCl rejection at 99.7%. However, the water flux was severely reduced. On the other hand, no significant improvement in terms of antifouling behaviour was observed. In fact, on increasing the concentration of the nanosheets, severe deterioration of the membrane performance was observed, mainly due to aggregation and localised defects formed on the PA layer.

To overcome the compatibility issue, research works focused on tailoring the g-C_3N_4 nanosheets with desirable functional groups and improving the dispersion in the monomer phases. Acidified g-C_3N_4 (aCN) nanosheets were incorporated into the PA layer to fabricate TFN membranes with higher water permeance and antifouling performance (Table S1, ESI,† entry 9).[69] aCN nanosheets had smaller size and higher solubility in water than g-C_3N_4 nanosheets. aCN incorporated TFN membranes at 0.005 wt/v% concentration showed superior RO performance. The water permeance was enhanced by 78.98% from 1.57 to 2.81 L m^{-2} h^{-1} bar^{-1}, compared to control membrane along with salt rejection at 98.6% for NaCl. The 2D planar structure of the nanosheets with distributed triangular pores and generation of nanovoids between nanosheets and the polymer matrix improved the water permeance. The rejection performance did not deteriorate much as the concentration of nanosheets was very low and did not impact the polymer structure. The membranes also showed superior antifouling performance against BSA and HA foulants. However, the membrane surface characterization revealed that there was no difference in the contact angle and surface zeta potential between the membranes incorporated with aCN and g-C_3N_4 nanosheets. It was suggested that the aCN nanosheets had higher dispersion capability in the aqueous solution when compared to g-C_3N_4, which resulted in smoother membranes which enhanced performance, but still the impact of nanosheets on the surface properties is unclear in this study.

The edges of g-C_3N_4 nanosheets could be attached to functional groups such as –COOH, –OH or SO_3H to further improve the hydrophilicity and surface charge. These hydrophilic functional groups would also facilitate uniform dispersion and good compatibility with the PA matrix. Accordingly, a study reported synthesis of three types of g-C_3N_4 nanosheets surface-functionalized with –COOH, –OH, and SO_3H respectively with the help of oxygen donor compounds (Table S1, ESI,† entry 10).[70] These nanosheets were

incorporated into the PA layer during IP reaction. The membranes incorporated with functionalized g-C_3N_4 nanosheets exhibited enhanced permeance without significant decrease in salt rejection. The membranes modified with 0.05 wt% choloroacetic acid-assisted functionalized carbon nitride nanosheets (g-C_3N_4-COOH) exhibited 54% increase in water permeance compared to g-C_3N_4 incorporated membranes, and high salt rejection of 98.1% of NaCl. In general, the membranes incorporated with these functionalized g-C_3N_4 nanosheets had higher surface negative charge and smoother surface due to the presence of hydrophilic functional groups and formation of hydrogen bonds with water molecules. The functional groups dissociated to impart high negative charge to the PA layer and thus enhanced the salt rejection and fouling resistance.

Another study incorporated polydopamine modified graphitic carbon nitride nanosheet (PDA-g-C_3N_4) into the active layer to fabricate a positively charged NF membrane.[71] Incorporating 0.005 wt% of PDA-g-C_3N_4 nanosheets decreased the surface roughness of the membrane, while increasing hydrophilicity and permeation. The membrane exhibited high rejections $>85\%$ for divalent cations (Mg^{2+}, Ca^{2+}, Ba^{2+}, and Cu^{2+}), while on the other hand the rejection of monovalent cation (Li^{+}) was low (36.8%). The membrane also showcased good antifouling properties. The fabricated membrane exhibited high potential for treatment of industrial wastewater and especially in separation of monovalent and multivalent ions.

Antifouling and chlorine-resistant properties of TFN RO membranes incorporated with g-C_3N_4 were reported in a recent study (Table S1, ESI,† entry 11).[17] At an optimized g-C_3N_4 concentration of 0.01 wt/v%, the pure water permeance increased by 30% and NaCl rejection was 99.23%. Total fouling rate decreased from 31.2% for the control PA membrane to 18.3% for the TFN membrane. Moreover, the TFN membrane showed higher chlorine resistance, with salt rejections decreasing by 1.08% compared to the 2.95% decline for the control membrane. However, compared to other membranes, the permeance of the TFN membrane was very low. The hydrophilicity and charge properties imparted are not conclusive and its performance enhancement needs to be established. To enhance the membrane performance a study simultaneously incorporated two nanofillers with different dimensions.[72] g-C_3N_4 nanosheets and halloysite nanotubes (HNTs) were co-deposited on the substrate membrane *via* vacuum filtration of aqueous solution containing PIP monomers and the nanomaterials, followed by the PA layer formation *via* IP reaction (Table S2, ESI,† entry 7). The integration of g-C_3N_4 and HNTs in the membrane structure resulted in a synergetic effect of the nanomaterial functionalities, which ultimately improved the membrane performance. The g-C_3N_4 nanosheets formed nanoaggregates which were enveloped by the PA layer over it and the HNTs were aligned horizontally, playing the role of a hydrophilic interlayer. This synergetic effect led to a crumpled membrane surface, additional water transport pathways, enhanced hydrophilicity and surface roughness. At an optimum concentration of 16.4 μg cm^{-2} of g-C_3N_4 and 19.7 μg cm^{-2} of HNTs in the aqueous phase, water permeance rose to 20.5 L m^{-2} h^{-1} bar^{-1}—a nearly two-fold increase when compared to the control membrane, with salt rejection at 94.5%.

2.3. BN-Incorporated TFN membranes

Boron nitride (BN) is an attractive 2D nanomaterial for application in high performance membrane filtration due to its exemplary properties such as chemical inertness, high strength, mechanical and thermal stability.[73–75] Hexagonal boron nitride is isostructural to graphene and often called white graphene.[74] The pioneering work of incorporating BN nanosheets into the PA layer for TFN membrane was done in 2018.[9] In the study, highly hydrophilic amine functionalized BN nanosheets (BN(NH_2)) were incorporated into the PA layer (Table S2, ESI,† entry 8). Incorporation of 0.004 wt% of BN(NH_2) into the PA improved the negative charge and hydrophilicity of the membrane surface, which resulted in 13.4% enhancement in permeance while maintaining high rejections for NOM. The addition of BN(NH_2) nanosheets into the aqueous phase influenced the IP reaction, impacting the PA layer morphology and chemical properties. When compared with the commercial NF270 and NFT50 membranes in terms of UV_{254} rejection, the TFN membrane performed well with the highest rejection of 97.91% whereas the values of commercial ones were 92.44% and 92.94% respectively. But though the NOM removal was very good when compared to commercial membranes, salt rejection studied with Na_2SO_4 solution yielded a lower rejection of 68.93%, which is undesirable. The rejections of $MgSO_4$ and NaCl were only 61.12% and 12.97% respectively. This reduced salt rejection was attributed to the looser PA layer with wider pathways for transport. As the concentration of nanosheets was increased, they tended to aggregate and lead to deterioration of performance. It was also observed that at concentrations lower than 0.008 wt% of BN(NH_2) nanosheets the contribution to the PA network was mostly though NH_2 functionalities and not *via* covalent bonding between C-*B*-N atoms. Hence, the presence of amine groups overshadowed BN nanosheets and their properties.

To further exploit the exceptional features of BN(NH_2) nanosheets, the nanosheets were coated on the PA layer, through covalent interactions.[45] Membranes decorated with 0.003 wt% BN(NH_2) nanosheets were reported to enhance the permeance by 59% and total fouling resistance by 50% when compared to control membrane (Table S2, ESI,† entry 9). BN(NH_2) decorated membrane showcased good stability during long term experiments. The TFN membrane possessed higher hydrophilicity, negative charge, and mechanical stability than the control membranes. Owing to these superior properties, during filtration studies involving BSA and SA, the normalized flux of BN(NH_2)-decorated membrane was at 95% after SA filtration and 99% after BSA filtration when compared to the control membrane with 79% and 92% respectively after 6 h experiments. Fouling-cleaning studies confirmed the enhancement of fouling resistance as the membrane showed very good flux recovery with lower fouling tendency than the control membrane due to the superior properties imparted by the BN(NH_2) nanosheets.

To check its real-world application, surface water samples from a reservoir were used as a feed and spectroscopic studies

were used to analyse the rejection properties.[11] The membrane was fabricated with modified IP process (PPA-BN) in which the nanofillers were incorporated into the PA layer and decorated over the PA layer (Table S2, ESI,† entry 10). The PPA-BN membrane displayed 69% higher permeance and exhibited improved NOM removal. Recent research has evaluated the performance of the BN nanosheet-incorporated TFN RO membrane.[76] The incorporation of nanosheet resulted in improved membrane surface hydrophilicity and roughness, which enhanced the water permeance by 25% with 96.4% rejection for NaCl (Table S1, ESI,† entry 12). However, the flux enhancement when compared to other TFN membranes was very low. The resultant TFN membrane exhibited excellent antifouling performance when compared to the control membrane. The membrane demonstrated improved chlorine tolerance due to additional amide bonds and crosslinking PA structure provided by the BN nanosheet.

2.4. MoS_2 incorporated TFN membranes

Transition metal dichalcogenides (TMD) are emerging 2D nanosheets in the field of water treatment owing to their distinctive physical and chemical properties.[26,77] TMD structure consists of a transition metal layer sandwiched between two chalcogen layers.[77] MoS_2 is a typical TMD consisting of hexagonal layers of Mo and S atoms. The MoS_2 sandwiched structure is shown in Fig. 1b. MoS_2 nanosheets have shown promise in membrane technology due to their distinctive properties such as mechanical strength, electronegativity and hydrophilicity.[78,79] MoS_2 exhibited reduced resistance for transport of water molecules due to its smoother surface and absence of oxygenated functional groups.[80] The presence of sulphur atoms on both sides of the MoS_2 layer aided hydrophilicity and provided higher affinity to water by means of hydrogen bonding. The first research work of incorporating MoS_2 nanosheets *via* IP reaction was undertaken in 2019 to fabricate TFN RO membranes.[78] At an optimum concentration of 0.01 wt% of MoS_2 nanosheet in the organic phase, flux and NaCl salt rejection properties of the membranes were improved to 6.2 L m^{-2} h^{-1} bar^{-1} and 99% respectively (Table S1, ESI,† entry 13). Increased concentration of MoS_2 nanofillers improved salt rejection, contrary to the fact that at higher concentration the nanosheets tend to form defects due to aggregation which leads to deterioration in salt rejection.[9,76] Incorporation of MoS_2 nanosheets enhanced separation performance due to its electronegativity, repelling the salt ions and facilitated higher rejection. Moreover, hydrophilicity of the membrane surface was greatly enhanced. Together, these effects resulted in simultaneous increase in water flux, salt rejection and fouling resistance. However, these membranes suffered leaching of the nanosheets during the first 2 h of experimentation, raising health concerns. The reason for leaching is suggested to be lack of functionalities on the nanosheets, causing poor interaction and compatibility with the polymer matrix. In another study, MoS_2 nanosheets were utilized to fabricate TFN NF membrane, overcoming the trade-off in permselectivity (Table S2, ESI,† entry 11). At an optimum concentration of 0.01 wt/v% in the organic phase, water permeance was increased by 2.5 times maintaining high salt rejection properties.[14]

To tackle the compatibility and stability factors, several additional studies were conducted to prepare functionalized MoS_2 nanosheets.[79,81–83] Accordingly, high efficiency polyphenol assisted liquid exfoliation was used as a green method to produce layered MoS_2 nanosheets with tannic acid (TA-MoS_2).[83] Due to their improved stability and compatibility, TA-MoS_2 nanosheets were successfully incorporated into the polyamide layer, forming a TFN NF membrane with superior performance. The optimum dosage of nanosheets was found to be 0.025 wt%, which enhanced membrane hydrophilicity and negative charge, and resulted in superior nanofiltration performance and long-term stability (Table S2, ESI,† entry 12).[84] The TFN membrane exhibited enhanced water permeance as high as 17 L m^{-2} h^{-1} bar^{-1}, with salt rejection maintained at 98.5% for Na_2SO_4. The study also confirmed that the nanosheets did not aggregate within the PA layer and exhibited high compatibility with the polymer matrix due to the functional groups on the 2D nanosheets. Non-selective defects were reduced due to high cross-linking sites available on TA-MoS_2 nanosheets, which in turn improved salt rejection. However, the increased surface roughness caused more fouling compared to control membrane.

To further improve the properties of MoS_2 nanosheets, TA-Fe^{3+} coordination complexes were used to modify MoS_2 nanosheets.[85] It was observed that TFN membranes incorporated with 0.01 wt% MoS_2–TA-Fe^{3+} demonstrated 1.6 times higher water permeance at 7.6 L m^{-2} h^{-1} bar^{-1} when compared to the control membrane, while retaining 96.5% salt rejection for Na_2SO_4(Table S2, ESI,† entry 13). This study also mentioned that the functionalization of the nanosheets increased the crosslinking sites for unreacted TMC molecules during IP reaction and simultaneously restricted the formation of interfacial voids. While studies of TFN membranes incorporated with MoS_2, showed that the hydrophilicity, surface roughness, PA layer thickness and crosslinking degree were all enhanced, this study found that TFN membranes incorporated with MoS_2–TA-Fe^{3+} displayed altered efficiencies. Incorporation of MoS_2–TA-Fe^{3+} nanosheets significantly affected surface roughness, and these membranes showed decreased hydrophilicity. This was attributed to the increased crosslinking degree which reduced the unreacted acid chloride groups on the membrane surface. While this effect did not significantly change the salt rejection, it would deteriorate antifouling performance which is highly dependent on the membrane hydrophilicity and charge. In addition, at concentration higher than 0.01 wt%, the membrane exhibited severely declined flux due to reduced hydrophilicity and increased crosslinking degree. When compared to other TFN membranes, the permeance was observed to be low.

A recent study incorporated oxidised molybdenum disulfide (O-MoS_2) into the polyamide active layer to form a TFN NF membrane (Table S2, ESI,† entry 14).[12] MoS_2 nanosheets were produced *via* exfoliation and oxidised by the Hummers' method. O-MoS_2 at an optimum concentration of 0.01 wt/v% dispersed in the organic phase showed exceptional performance, with 2.5-fold higher permeance with good antifouling properties. The rejection of Na_2SO_4, $MgSO_4$, $MgCl_2$ and NaCl were 97.9%, 92.9%, 86.3% and 65.1% respectively, which was comparatively higher than the

value for the control membrane, as a result of the reduced pore size and higher negative charge on addition of O-MoS_2. The reduction in pore size was attributed to the increased density of the PA layer on addition of O-MoS_2 nanosheets as well as the partial coverage of the pores by the nanosheets.

2.5. Other emerging nanosheets-incorporated TFN membranes

Transition metal carbides and nitrides (MXenes) nanosheets based applications have been hot topic of research since its discovery in 2011. MXenes are described by the general formula $M_{n+1}X_nT_x$ (n = 1–3), where M is an early transition metal, X represents carbon and/or nitrogen, T denotes functional groups (OH, O, Cl, or F) and x represents the number of these groups. MXenes are derived from selective etching of precursors represented as MAX ($M_{n+1}AX_n$), where A is usually an element from groups 12–16.[16,86–89] Until now, around 30 MXene compounds have been synthesized from MAX precursors.[90] Among them, Titanium-based MXenes, particularly $Ti_2C_2T_x$ and $Ti_3C_2T_x$, have been explored for environmental remediation applications.[89,90] MXenes possess excellent features such as high hydrophilicity, high surface area, activated hydroxide sites, ease of functionalization combined with adsorptive, anti-bacterial and metallic properties, which facilitate their utilization in membranes for water treatment applications and electrokinetic power generation.[87,90–92] Recent studies have showed promising results for MXene-based membranes with high flux, rejection properties, antifouling performance, and anti-bacterial properties.[86,88,93–97]

The role of MXene nanosheets in improving TFN membranes was explored recently. The study incorporated $Ti_3C_2T_x$ into the PA layer to fabricate TFN RO membranes (Table S1, ESI,† entry 14).[16] $Ti_3C_2T_x$ was synthesized by selective etching of Al from the precursor Ti_3AlC_2 using hydrogen fluoride. $Ti_3C_2T_x$ was dispersed into the aqueous solution and incorporated into the PA layer during IP reaction at various loadings ranging from 0–0.02 wt%. This led to the formation of a PA layer with lower surface roughness, lower thickness and higher hydrophilicity which translated into higher flux (2.3–2.5 L m^{-2} h^{-1} bar^{-1}) when compared to the control membrane (1.7 L m^{-2} h^{-1} bar^{-1}), while the salt rejection (97.9–98.5%) was similar to that of the control membrane (98.6%). Antifouling experiments with BSA confirmed that at a concentration of 0.015 wt% of $Ti_3C_2T_x$, the membrane showed superior fouling resistance with low flux decline value of 11.11% after 6 h when compared to 22.72% of the control membrane.

COF nanosheets have been explored for their application in water treatment and especially in membrane-based separations.[98,99] COF nanosheets are emerging microporous crystalline materials which are synthesized from organic linkers. Recently, COF has received tremendous research attention in membrane separation due to its superior properties such as large surface area, high crystallinity, uniform and tuneable pore structure, versatile covalent building blocks, attachment of various functional groups, and excellent thermal and chemical stability.[28,99] A novel TFN RO membrane was fabricated by incorporating COF nanosheets with high crystallinity, achieving superior water/NaCl selectivity. Novel COF (TpPa) was synthesized *via* microwave-assisted Schiff-base reactions.[18] TpPa nanosheets were dispersed in the aqueous phase containing MPD monomer. The IP reaction scheme was facilitated by the vacuum filtration method. The resultant TFN membrane incorporated with 50 μg cm^{-2} TpPa nanosheet exhibited three-fold water permeance at 2.2 L m^{-2} h^{-1} bar^{-1} compared to the control membrane and retained 97.7% salt rejection for NaCl (Table S1, ESI,† entry 15). TpPa nanosheets improved the hydrophilicity, negative charge and surface roughness of the membrane, which together improved the water permeance. The electronegative nature of the TpPa nanosheet resulted in lowered NaCl permeance, improving the water/NaCl selectivity. The higher chlorine resistance was attributed to the amide and methyl groups present in the COF.

A recent study reported a unique method of stitching COF-based nanosheets to build aligned nanopores for NF membranes (Table S2, ESI,† entry 15).[100] Amino-functionalized nanosheets (TpBD-NH_2) were synthesized by solvothermal synthesis followed by chemical reduction. The nanosheets were stitched at the oil–water interface to form fishnet-like nanofilm structures with TMC molecules. These nanofilms were encapsulated into the PA layer during the IP reaction. The nanofilms induced aligned pores and controlled the PA layer formation. The nanosheets were covalently bonded into the matrix, enhancing their compatibility with the polymer. The oriented pores promoted controlled diffusion of PIP molecules and facilitated formation of thinner PA layer with patterned surfaces. The resultant membranes showed enhanced permeance and selectivity for both monovalent and divalent salts. However, this novel TFN membrane exhibited lower water permeance at 6.0 L m^{-2} h^{-1} bar^{-1} when compared to the membrane incorporating the COF nanosheets in PIP solution, at 9.5 L m^{-2} h^{-1} bar^{-1}.

Metal organic frameworks (MOFs) is an emerging nanomaterial currently explored for various applications such as adsorption,[101] catalsysis,[102,103] electrochemical sensing,[104] energy storage/conversion,[105,106] and membrane separation processes.[31,107] MOFs are crystalline porous materials comprising of metal ions/clusters as building blocks linked by organic ligands.[101] MOFs possess very high surface area and porosity, tuneable structure, pore size and surface morphologies, and capacity to be combined with several functional groups.[103] The presence of organic linkers and functional groups could facilitate the compatibility of the MOFs within the polymer matrix. TFN membranes incorporated with MOFs such as zeolitic imidazolate framework-8 (ZIF-8),[108,109] zirconium based MOF (UiO-66),[110] and various other zinc based,[43,111] chromium based[112] and copper based MOFs have exhibited enhanced separation performance.[113] However, it is a great challenge to synthesize 2D MOFs with atomic thickness, suitable structures and tuneable properties in large scale. In addition, MOFs also suffer stability issues leading to structural deterioration.[101,107] The interaction of MOFs with polymer network would depend on the type of MOFs and its functionalities, which can be used to manipulate the selective PA layer and separation performance of the membranes. There needs to be conclusive study on impact of 2D MOFs nanosheets on the membrane performance.[114] However, 2D MOFs synthesis and

incorporation into TFN membranes for water treatment applications would be an exciting research field due its versatility and different possible MOFs structures.

3. Impact of 2D nanosheets on PA layer and membrane performance

Apart from acting as alternate transport pathways for water molecules, 2D nanosheets impact the properties and formation of the PA layer of the TFN membranes conclusively enhance the membrane performance. They influence the IP reaction through their impact on reaction interface, diffusion of amine monomers, and the confinement effect of degassed nanobubbles. Their surface charge, size and hydrophilicity improve the reaction interface and facilitate the IP reaction. In addition, they also impact the interfacial stability and the IP reaction rate. For instance, NH_2 groups present on BN nanosheet react with TMC, forming more amide bonds and improving the membrane rejection performance. 2D nanosheets also facilitate formation of cross-linked PA structure, which leads to reduced pore size, improving the rejection properties of the TFN membrane.[12,85] The presence of 2D nanosheets during the IP reaction also affects the diffusion rates of the amine monomers. The concentration of PIP or MPD is the rate limiting factor, as the diffusion occurs from the aqueous to organic phase. 2D nanosheets have demonstrated both controlled release and enhanced sorption of amine monomers during IP reaction. Reduced diffusion rate of amine monomers has been recorded in various studies.[9,85] For instance, incorporation of mGO nanosheets comprehensively reduces the diffusion rate of MPD molecules into the organic phase.[54] The combined effect of steric hindrances and chemical interactions of the functionalities on the nanosheets impacts the reaction rate between MPD and TMC. The carboxyl and hydroxyl groups of the mGO structure particularly also interact with TMC, affecting the IP reaction. As a result of these interactions, a thinner PA layer is formed, which reduces the resistance to water transport, thus enhancing the water permeance of the membrane. From cross-sectional SEM morphologies of the control and mGO-incorporated membranes in Fig. 2a, it is evident that the thickness of the PA layer has decreased drastically from 240 nm to 50 nm when the loading of mGO was increased from 0 to 0.005 wt%. The nanosheets also lead to formation of leaf-like structures on the surfaces of TFN membranes when compared to nodular structures in the control membrane. Indeed, many studies confirm that 2D nanosheet incorporation leads to the fabrication of TFN membranes with a thinner and smoother PA layer. The smoother surface also facilitates lower fouling tendency as it provides fewer attachment sites for foulants.[16,46,70]

The incorporation of MoS_2–TA-Fe^{3+}nanosheets however shows crumpled structures with scattered tufts.[85] The MoS_2–TA-Fe^{3+} nanosheets attract PIP monomers through hydrogen bonding interactions in the aqueous phase. This local enrichment effect of PIP molecules facilitates their diffusion during the IP reaction, leading to protruding structures on the membrane surface. Increasing concentration of nanosheets during the IP reaction hinders the diffusion of aqueous monomers and leads to the formation of a smoother membrane surface with thinner PA layer. However, addition of the nanosheets beyond the optimum concentration negatively affects the membrane structural integrity and reduces both the permeance and salt rejection performance.[9] The incorporation of MoS_2 nanosheets at low concentrations facilitates uniform distribution over the PA layer.[78] As the concentration is increased, the nanosheets tend to aggregate and cover the PA layer as shown in Fig. 2b, deteriorating its performance.

In terms of surface roughness of the TFN membranes, both increasing and decreasing trends have been reported by several studies.[9,11,16,18] The increase in surface roughness is on account of the confinement effect of the gas bubbles produced during the IP reaction.[44] The IP reaction leads to formation of CO_2 bubbles which are released through the PA layer. The encapsulation of the nanosized gas bubbles into the PA layer caused due to the influence of nanosheets, leads to the formation of nanovoids and leaf-like structures along with the conventional ridge-valley protuberances in the PA layer.[115] In addition, the functionalities attached to the nanosheets also take part in the IP reaction and act as alternate reaction pathways, causing increased surface roughness.[9,84] The NH_2 and COOH groups present on g-C_3N_4 react with TMC molecules, leading to ionic interactions and wrinkling effect of the polymeric chains which caused significant increase in surface roughness.[17] Increased surface roughness increases the filtration area, leading to formation of a water hydration layer on the surface, which improves water permeance and prevents deposition of organic foulants. However, this effect can also lead to trapping and accumulation of foulants in the rough microstructures, causing deterioration of the membrane performance.[11] In a few other studies, surface roughness was observed to reduce when nanosheets were incorporated into the PA layer.[18,68,70] The intrinsic hydrophilicity of g-C_3N_4 nanosheets and the tendency of the triazine units to form hydrogen bonding with OH^- ions present in the polymerization solution leads to reduced roughness.[68] In addition, the functional groups present on the nanosheets also form hydrogen bonds with amine groups of the monomer. This leads to a compaction effect on the molecular chains, causing a smoother surface.[70] Nevertheless, the surface chemical characteristics such as hydrophilicity and charge density also majorly impact the membrane performance.[11] The intrinsic hydrophilicity of the incorporated 2D nanosheets alter the hydrophilicity of the PA layer formed. The PA layer with higher hydrophilicity enhances the solubilisation and diffusion of water molecules through it, improving permeance.[76]

Hydrophilicity is also dependent on the surface roughness of the PA layer formed. The higher the surface roughness, the lower the contact angle and improved hydrophilic membrane.[12] The tendency of the functional groups attached to the nanosheets to form hydrogen bonds also enhances the hydrophilicity of the PA layer in many cases.[9,16,45,70] Hydrophilicity of the membrane surface can decrease the deposition of hydrophobic organic foulants and improve the antifouling performance of the membranes.[9,13,51,67] The influence of nanosheets on hydrogen bonding with amine monomers and the reduced diffusion

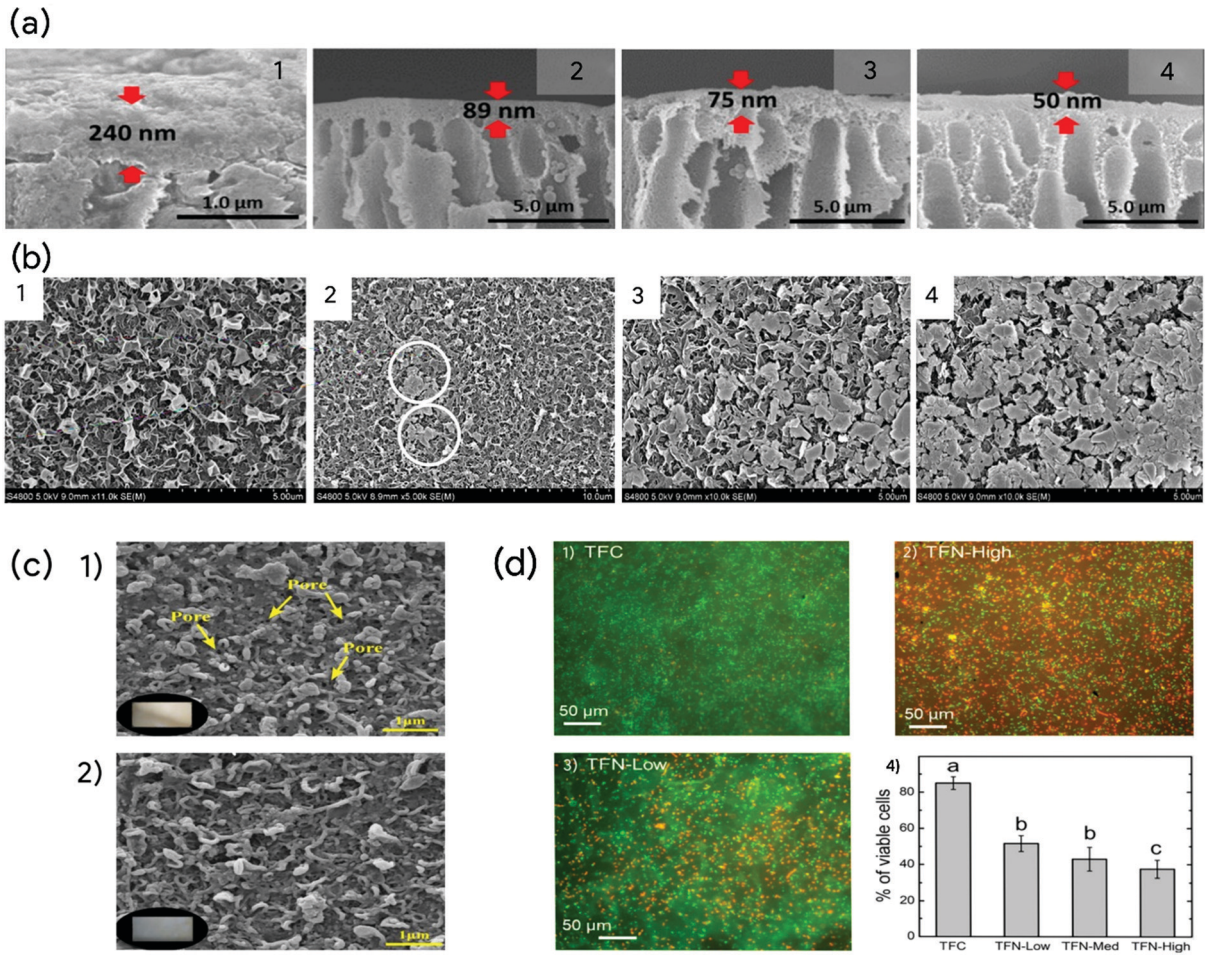

Fig. 2 (a) Cross-sectional SEM images of control and TFN membranes incorporated with 0.002 wt%, 0.003 wt% and 0.005 wt% mGO respectively (1–4), Adapted with permission.[54] Copyright 2019 Elsevier. (b) SEM surface morphologies of control and TFN membranes incorporated with 0.005 wt%, 0.02 wt% and 0.05 wt% MoS_2 respectively (1–4), Adapted with permission.[78] Copyright 2018 Elsevier. (c) SEM surface morphologies (1–2), of PA and 0.015 wt% $Ti_3C_2T_x$ incorporated PA15 membranes after chlorine exposure test, Adapted with permission.[16] Copyright 2020 Elsevier. (d) Epifluorescence microscopy images of *E. coli* cells on control TFC (1), TFN-Low (2) and TFC-High (3). Green and red colour represents live and dead cells, respectively. (4) Cell viability of adhered *E. coli* cells after 3 h of contact. Adapted with permission.[46] Copyright 2018 Elsevier.

towards the organic phase increases the quantity of free acyle chloride groups on the membrane surface. These groups enhance the surface negative charge due to the formation of carboxylic moieties. The intrinsic charge properties of the nanosheets also impact the surface charge of the membranes. In the case of BN nanosheets, the electron deficient nature of B atoms, Lewis acidity and their propensity to acquire OH^- ligands in water enhances the negative charge density.[45] The enhanced negative charge facilitates higher salt rejection and antifouling effect due to the electrostatic interactions.[12,76,78] Due to the interaction during IP reaction, the nanosheets also enhance the density of the PA layer formed and reduce the pore size. The partial coverage of the pores due to the horizontal placement of the nanosheets over the pores also contributes to the reduction in its size.[12,45] Reduced pore size along with selective rejection of salt ions through the intrinsic pores of the nanosheets also contributes to enhancement of salt rejection.

When the 2D layered nanosheets are incorporated into the TFN membranes, they are proposed to contribute to the formation of additional water transport mainly through two mechanisms. In the first mechanism, interfacial voids are formed between the PA network and 2D nanosheets which offered lower resistance to water transport leading to quick selective transport of water molecules.[9,68] As the size of nanovoids increases, the passage of both water molecules and salt ions are possible which deteriorates the salt rejection performance of the membranes.[116] However, there are no conclusive evidence through SEM images. It is also argued that such interfacial voids cannot be detected by electron microscopic imaging, but would contribute to the water permeance.[30] In the second mechanism, the intrinsic nanovoids present on the 2D nanosheets and the interlayer spacing facilitates selective transport of water molecules through its nanochannels enhancing the water permeance.[68] The interlayer spacing and nanovoids can be influenced by the synthesis method and functionalisation of nanosheets to achieve desired separation performance.[51]

The comprehensive influence of the nanosheets also improves the mechanical, chemical, and thermal stability of the TFN membranes.[45,52,72] BN nanosheets enhanced the tensile strength

and breaking elongation of TFN membrane.[45] The mechanical strength and wrinkled topology of BN nanosheets causes mechanical interlocking and reinforced polymer structure. This reinforced polymer structure exhibited stable filtration performance during 52 h operational stability experiments. Similarly, TFN membrane incorporated with GO showed stable performance during a 72 h extended filtration process, due to the mechanical strength imparted by GO.[52] It is well noted that GO-incorporated nanocomposites have showed enhanced reinforcement of the matrix, leading to very high strength and toughness.[117] Another important feature bestowed by nanosheets is improved chlorine resistance of the membranes. Several studies have reported their shielding effect on the vulnerable amide bonds during chlorine exposure tests. The combined effect of enhanced cross-linking and interactions of functional groups reduces the impact of chlorine attack on the PA layer. For instance, $Ti_3C_2T_x$-incorporated TFN membranes after exposure to 5 cycles of 2000 ppm NaOCl chlorination exhibited increased water flux with high salt rejection.[16] As shown in Fig. 2c, the morphological observations of the control PA and TFN membranes suggest high yellowing degree and visible exposure of pores on the control membrane. The amide bonds in the PA layer are damaged, leading to deformation of the layer, causing defects and micro voids in its structure, leading to increased permeance and lower salt rejection.

From the aspect of tailoring the fouling resistance properties, the combined impact of surface hydrophilicity, negative charge density, and steric hindrances plays a huge role in decreasing the fouling propensity of the TFN membranes in contact with organic and biological species.[9,11,46,54,58] As discussed previously, the surface hydrophilicity, increase in the number of hydrogen bonds and the electrostatic interactions can lead to the formation of a water hydration layer over the membrane surface which prevents the attachment of organic foulants. In addition, as a result of the steric hindrance and electrostatic repulsion effects owing to the distribution of nanosheets over the PA layer, the foulants are pushed away, minimizing their adsorption on the surface. Membranes incorporated with BN nanosheets exhibited lowest fouling and decline of flux to 80%, compared to 54% for the control PPA membrane. The commercial XN45 membranes exhibited very high flux decline within the first few hours of the experiments. PPA-BN membranes showed most stable performance at the beginning and throughout the 52 h test, due to their surface hydrophilicity and surface charge. Greater initial fouling of the membranes leads to irreversible entrapment of the foulants on the surface, necessitating intermittent chemical cleaning to recover partial value of initial flux. On the other hand, during the filtration experiment PPA-BN membranes exhibited gradual flux decline due to the formation of a loose organic fouling layer which is susceptible to physical cleaning. PPA-BN membranes also performed well at low pH and high Ca^{2+} concentration in feed water.[11]

Polymeric membranes are also prone to biological attacks due to the availability of organic moieties such as proteins and carbohydrates near the membrane surface. This facilitates the adhesion, proliferation, and metabolism of microbes, resulting in the forming of biofilms on the membrane surface. In addition, the formation of extracellular polymer substances acts as a shield to protect them.[118] The microbes also facilitate the deposition formation of minerals, leading to mineral scaling combined with biofouling.[119] Available literature suggests that incorporation of the 2D nanosheets, particularly GO, reduces the biofouling tendency to a great extent.[46,49,54] One strategy to mitigate biofouling is to ensure reduction of the cell adhesion through improved surface charge, hydrophilicity, and smoother surface of the membrane.[49] In addition, the incorporation of biocides such as Ag^+ and Cu^{2+} on the GO structure makes microbes inactive by effectively reacting with their cell walls and DNA.[58,60] The reactive oxygen species formed by the biocides causes oxidative stress in the cells and also breaks down their proteins, damaging them.[120] In a particular study, TFN membranes incorporated with GO nanosheets, TFN-Low, TFN-med and TFN-High decreased the cell viability to 52%, 43% and 37% respectively when compared to 85% for the control TFC membrane as Fig. 2d.[46] The intrinsic biocidal nature of GO and the sharp edges of the nanosheets resulted in reducing the cell viability and biofilm volume.

4. Potential for 2D-enabled TFN membranes for water purification and desalination application

TFN membranes with high water permeance and good selectivity find use in a wide range of applications for freshwater production. The applications include desalination of sea water and brackish water, drinking water treatment, industrial wastewater treatment and reuse, and resource recovery. Water permeance and salt rejection of these membranes are highly dependent on the type of nanosheets used and their impact on the PA layer properties. For both RO and NF, membranes displaying high water permeance and salt rejection are desirable. Tables S1 and S2 (ESI†) summarizes the water permeance, salt rejection and the impact of 2D nanosheet on the physicochemical properties and performance of 2D-enabled TFN membranes discussed in the paper. The trend observed from Fig. 3a infers that GO incorporated TFN membranes characteristically have lower water permeance and weak impact on the salt rejection capabilities. The variation in permeance and rejection properties for g-C_3N_4 embedded TFN membranes are due to the influence of different functionalities attached to the 2D nanosheets. g-C_3N_4 incorporated TFN membrane exhibited very high salt rejection at 99.7% with no improvement in water permeance against control membranes.[68] MoS_2-enabled TFN membrane showcased the highest water permeance at 6.2 L m^{-2} h^{-1} bar^{-1}, while maintaining high selectivity with 99% salt rejection.

Permeance for commercial RO membranes is in the range 1–2 L m^{-2} h^{-1} bar^{-1} for seawater RO and 2–8 L m^{-2} h^{-1} bar^{-1} for brackish water RO (BWRO), with salt rejection $>99.9\%$ and 95–99% respectively.[121,122] Several studies have reported that increase in water permeance of the RO membranes can possibly reduce the specific energy consumption of the process, depending upon the model assumptions and operating conditions.[123–125]

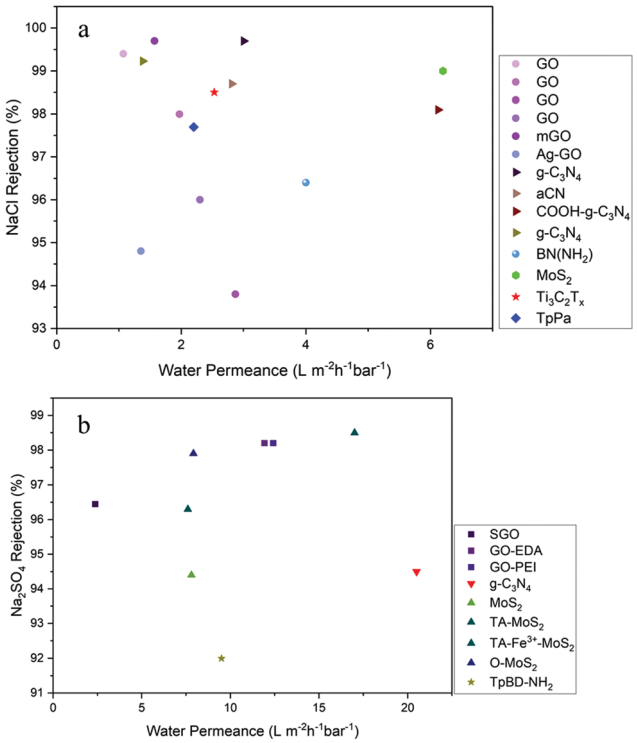

Fig. 3 Performance of 2D-enabled TFN membranes for (a) NaCl rejection and (b) Na_2SO_4 rejection.

Despite enhanced permeance at 15 L m^{-2} h^{-1} bar^{-1} for the TFN membrane, the specific energy consumption predicted was reduced by a mere 16.6% when compared to commercial TFC membrane with 1 L m^{-2} h^{-1} bar^{-1} permeance.[44] From the marginal reduction in this case, it is evident that energy consumption is more dependent on the osmotic pressure of the feed and the operating conditions rather on permeance. It was observed that energy consumption reduces for operations such as BWRO and NF membranes operating at 5–10 bar pressure. The same study found that use of TFN membranes reduced the specific energy consumption >80% compared to the commercial BWRO membrane. It is worth noting that the energy calculation models have not considered the fouling effect and the ageing of the membranes during operation. Fouling decreases the flux of the membranes and deteriorates the performance and membrane integrity. In addition, increased permeance might also trigger more fouling due to concentration polarization. Therefore, membranes with enhanced antifouling properties are desirable. The antifouling performances of TFN membranes cannot be directly compared with each other due to the variation in experimental setups and operational parameters. Apart from the membrane surface characteristics, feed water chemistry and filtration conditions play a vital role in the deposition of foulants. Hence, future studies should follow a standard protocol for filtration tests in terms of membrane size, flow conditions, module setup, and feed water characteristics which can facilitate performance comparison. However, TFN membranes incorporated with 2D nanosheets have showed improved antifouling and biofouling resistance performance, which is highly favourable as it reduces the cost associated with frequent maintenance and replacement of the membranes.

From the context of NF, commercial membranes have a permeance in the range 5–12 L m^{-2} h^{-1} bar^{-1} with Na_2SO_4 rejection greater than 98%.[9,11,51] When compared to RO membranes, NF membranes have a looser PA structure with higher water permeance and lower operating pressure. NF membranes exhibit high rejection of small neutral molecules, organic entities and charged multivalent ions, while facilitating transport of water and monovalent ions. Fig. 3b depicts the permeance and rejection values of 2D-enabled TFN NF membranes. The functionalities present on the nanosheets greatly impacted the membrane permeance and rejection performances. Even for same parent 2D nanomaterial GO, the functionalization with sulfonic acid, EDA and PEI respectively resulted in variation in permeance ranging from 2–12 L m^{-2} h^{-1} bar^{-1}. Similarly, MoS_2 incorporated TFN membrane performance was impacted by the different functionalities attached to the 2D nanosheets. TFN membranes incorporated with TA-MoS_2 nanosheets showcased the highest salt rejection at 98.5% for Na_2SO_4, with water permeance at 17 L m^{-2} h^{-1} bar^{-1}. The membrane also exhibited good selective rejection to divalent ions over monovalent ions, with rejection for NaCl at 28%.[84] TFN membranes incorporated with O-MoS_2 showed water permeance improved by 155% from 3.11 to 7.91 L m^{-2} h^{-1} bar^{-1}, accompanied by high rejection of Na_2SO_4 at 97.9%.[12] The highest water permeance for 2D-enabled TFN NF membranes was exhibited by the membrane incorporated with g-C_3N_4 nanosheets, at 18.8 L m^{-2} h^{-1} bar^{-1} but with low salt rejection of 84% for of Na_2SO_4. However, the synergetic impact of g-C_3N_4 nanosheets and HNT showed high water permeance of 20.5 L m^{-2} h^{-1} bar^{-1} and Na_2SO_4 rejection of 94.5%. Separation of monovalent and multivalent ions was enhanced for membranes incorporated with PDA-g-C_3N_4. Salt rejection was maintained high for divalent ions including Mg^{2+}, Ca^{2+}, Ba^{2+}, Cu^{2+} and Zn^{2+}, and monovalent rejection was at 36.8% for LiCl.

BN-Incorporated membranes recorded low rejections for Na_2SO_4 ranging from 69% to 89% with good water permeance in the range 7 to 15 L m^{-2} h^{-1} bar^{-1}.[9,11,45] However, it is noteworthy that the membranes were optimized for organic removal and antifouling performance for filtration of surface water. Dual modified PPA-BN membranes with nanosheets—both in the PA layer and decorated over it—resulted in improved water permeance, NOM rejection, antifouling performance, and lower chlorine demand for the permeate.[11] PPA-BN membrane exhibited very high removal at 89% and 95% respectively for DOC and UV_{254} rejection, while commercial XN45 membrane had a rejection of 71% and 87% respectively. The high removal of NOM resulted in lower chlorine demand of the permeate, which reduced the formation of carcinogenic disinfection by products.

Most of the studies involving GO nanosheet-incorporated membranes discovered a trade-off between permeance and salt rejection, mainly due to the incompatibility of non-oxidized regions of the GO structure with the PA matrix, leading to formation of undesirable voids and defects which act as non-selective pathways.[84] Similar trade-off has been also observed

for TFN NF membranes incorporated with g-C_3N_4 and BN nanosheets.[9,67] The GO structure is also unstable when in contact with water and harsh chemicals, leading to degradation of membrane integrity and deterioration in performance.[52] A recent study concluded that incorporation of GO had greater impact on antifouling and antimicrobial performance than on permeance. At low concentration of GO, the membrane permeance was enhanced a little, but at higher concentrations the permeance decreased with stable salt rejection while the antifouling and antimicrobial performance was highly improved. Incidentally, production methods of GO nanosheets involve hazardous solvents and oxidizing agents which is unsustainable and impact the environment.

BN-Incorporated TFN membranes have shown excellent antifouling and organic removal performances. However, the salt rejection of NF membranes is very low, which is undesirable for both brackish groundwater and surface water desalination. The improvement in permeance is also lower when compared to other TFN membranes. Compared to other nanosheet fabrication procedures, BN is produced *via* a facile single-step ball milling technique. Besides, this is also is a green synthesis method which does not involve any toxic solvents.[9] Nanosheets produced thus have good functionalities and higher yield with low energy consumption. Membranes incorporated with MoS_2 show the potential to simultaneously increase flux and salt rejection, bridging the trade-off between permeability and rejection. However, the membrane permeance is lower than that of many TFN membranes available in the literature. Leaching of MoS_2 nanosheets was reported during the filtration experiments, which can impact the membrane performance negatively. In terms of the antifouling performance of TFN membranes incorporated with MoS_2, the results were highly impacted by the synthesis technique of MoS_2 nanosheets and the functional groups present on its surface. Nanosheets of TMDs such as WS_2 have been explored as membrane materials and can also play a role as nanofillers for TFN membranes.[126,127] Other emerging nanosheets such as MXene and COF are at a very primitive stage in research and development in terms of being used as nanofillers for TFN membranes. Their impact on the PA layer properties and membrane performance must be comprehensively evaluated and benchmarked against commercial membranes. Distinctive insights into the 2D nanosheet material-membrane properties and performances are tabulated in Table S3 (ESI†). 2D nanosheet-membrane relationship is highly influenced by the functionalities present on the nanosheets as they play an integral part in interacting within the polymer matrix governing its structure and chemistry.

5. Challenges and prospects

5.1. Challenges in manufacturing in design

Although 2D-enabled TFN membranes have showed enhanced performance, there are some critical challenges which need to be addressed. One major challenge is aggregation of nanosheets which leads to defects in the PA layer, negatively impacting the membrane separation performance. The major cause of this phenomenon is the poor compatibility of the nanosheets with the PA matrix. Low dispersion of the nanosheets in the monomer phases and their poor interaction during the IP reaction cause aggregation and irregular distribution over the PA layer. Hence, a few parts of the PA layer are devoid of the nanosheets in such cases, leading to compromised membrane surface and performance. In addition, this also leads to leaching of nanosheets from the PA layer during operation, which is a potential threat both to human health and the environment, combined with deterioration of membrane performance. To overcome this compatibility issue, nanosheets must be strongly bonded with the PA matrix chemically and have sufficient interactions with the polymer structure. This is achieved by introducing suitable functionalities on the nanosheets so that they are strongly anchored in the PA layer during the IP reaction. It is worth noting that, the functional groups present on the nanosheets highly influence the PA layer formation and the performance of the membranes. A general rule of thumb followed for TFN membrane fabrication is ultrasonication of the nanosheets dispersed phases prior to IP reaction. This is articulated to homogenize the solution and avoid any aggregation of nanosheets. IP reaction scheme has been conducted under ultrasonic environment to improve the interfacial mixing of monomers.[128,129] Similarly 2D-enabled TFN membranes can be fabricated under ultrasonic waves to enhance nanosheet mixing and PA layer formation.

The random distribution of nanosheets is exacerbated by the aqueous phase removal methods. Conventionally, after contacting the membrane with the aqueous phase, removal methods such as rubber roller, airgun or air knife are used. This can lead to loss of nanosheets, uneven distribution on the PA layer and undesirable defects which compromise the membrane integrity and separation performance. These techniques have poor reproducibility, and are prone to manual error.[130] Adding to this fact, the conventional removal techniques of excess monomers are not efficient, requiring more research interest in uniform and controlled removal of monomers from the substrate.

Recently IP reaction assisted by vacuum filtration, spin coating,[130] spray coating,[131] ultrasonic atomization[132] and electro spraying[133] has been developed for membrane fabrication, resulting in enhanced membrane chemistries and morphologies providing superior filtration performance and bridge the trade-off between permeance and selectivity. However, these methods are not cost-effective, and hard to scale up. Vacuum filtration and spin coating are viable for only a small membrane area and might lead to loss of nanosheets through the substrate pores, and during the spin operation in the case of spin coating. IP reaction assisted by spray and electrospraying techniques led to fabrication of membranes with precise control over the PA layer with minimum use of chemicals. However, they are energy intensive and time-consuming methods. In addition, the size and characteristics of nanosheets might be altered due to the spraying effect. Alternative options such as support-free IP technique,[134] reverse IP technique,[135,136] stitching of nanosheets prior to IP reactions[100] and nanosheets interlayer[43] have been explored to fabricate TFN membranes. Support-free IP technique suffers

from difficulties to attach or transfer the fabricated fragile PA layer onto the support membrane. Reverse IP is similar to the conventional IP technique with the sequence of contacting the aqueous and organic phase reversed. Defect free and controlled PA layer formation is difficult in this method. Stitching of nanosheets prior to IP and nanosheets interlayer techniques again involves vacuum filtration assistance restricting its scale-up option. In addition, the chemical interactions and stability of the interlayer with the PA layer needs further research.

The production of most nanosheets is costly and time consuming, and is accompanied by toxic wastes. The techniques involve complex procedures and require precise instrumentation. Yet, the volume produced is very low in most cases. In addition, the exfoliation of nanosheets is an energy-intensive process with financial implications. Besides, the methods also involve use of toxic solvents, leaving behind wastes which are hazardous to human life and the environment. Conclusively, the production methods are complex and difficult to scale up, thus restricting their actual industrial preparation and application. Production of GO is comparatively the cheapest among 2D nanosheets due to the cheap and abundant availability of the parent material—graphite. However, production of superior quality GO costs 390 US$ g^{-1} [137] while other 2D materials such as BN and MoS_2 are very expensive at 944 US$ g^{-1} [138] and 1216 US$ g^{-1} [139] respectively. It is worth noting that while 2D nanosheets such as BN, g-C_3N_4, MoS_2, MXene and COF have been able to enhance the performance of the membranes, the cost factor and environmental impact of their production and operation cannot be overlooked. The challenges associated with different 2D nanosheet-enabled TFN membranes are tabulated in Table S3 (ESI†). Aggregation of 2D nanosheets is an inevitable challenge observed in all 2D-enabled TFN membranes.

5.2. Future perspectives

2D nanosheets have unique properties based on their synthesis and functionalization, and care should be taken to understand the fundamentals of their properties and to exploit their full potential as nanofillers for TFN membranes. Their properties such as stability in water, dimensions, pore size, electrostatic charge, dispersion in polar/non-polar solvents and chemical interaction and orientation with PA layer must be taken into account to fabricate high performance TFN membranes with desirable properties. Tremendous research effort is needed to synthesize nanosheets with precise control over their dimensions, functionalities, and properties, in a cost-effective, environment-friendly, and scalable production method. Most of the techniques currently used for synthesis of 2D nanosheets involve highly toxic chemicals and show poor scalability. Replacement of toxic chemicals with green or relatively low toxic chemicals is desirable. Functionalities attached to the nanosheets are highly crucial in imparting good compatibility and strong anchoring with the polymer matrix. Simple and easy functionalization of nanosheets needs to be further explored. Sustainable plant-based monomers and solvents are emerging which are alternatives to existing petroleum-based ones which are toxic and hazardous.[140] However, further research is needed to find sufficiently reactive natural monomers and suitable green solvents with compatibility for incorporation of nanomaterials.

TFN membrane incorporated with GO has been the subject of major studies for antibacterial properties and biofouling resistance. Other nanosheets such as BN, MoS_2, g-C_3N_4, COF and MXenes should also be studied similarly. The synergetic effect of incorporating different 2D nanosheets or other additives simultaneously during IP reaction can also be explored. It is reported that the introduction of polyvinyl alcohol (PVA) in the aqueous phase during IP reaction, enhanced the dispersion and compatibility of GO resulting in fabrication of highly hydrophilic and defect-free membranes with improved antifouling performance and water permeance.[141] Similarly, synergetic impact of other additives along with 2D nanosheets could be explored. It has been observed that GO nanosheets have a greater impact on antibacterial properties than transport properties, while MoS_2 nanosheets provide enhanced permeation and salt rejection. How the synergetic effects of these two—or other—nanosheets influence the IP reaction and properties of the PA layer is also an exciting area of research. The antifouling strategies of 2D-enabled TFN membranes mainly focus on the surface charge and hydrophilic properties. However, further research can explore their photocatalytic behaviour and reactivity towards organics and fouling agents for application in self-cleaning membranes and membrane reactors.

Nevertheless, most TFN membranes are still at the lab-based research stage, involving ideal feed solutions and operation conditions for short durations. Most of the studies involving TFN membranes are focussing on desalination performance. Separation of emerging pollutants such as persistent organic pollutants, pesticides, pharmaceuticals, microplastics and per/poly fluoroalkyl substances (PFAS) should also be systematically studied, and performance optimized for pollutant-specific membranes. TFN membranes should be also examined for domestic and industrial wastewater treatment. The membranes must be evaluated for their performance in pilot scale plants and examined from an industrial perspective. Long-term experiments with multiple fouling-cleaning cycles must be carried out to understand the possible deterioration of performance and associated maintenance needed. It is also observed that, most production methods of nanosheets are costly, which increases the cost of manufacturing the membranes. Enhancement in membrane performance outweighing the associated cost factor would make these membranes viable. Hence, further studies should confirm the superiority of 2D nanosheets when compared to other additives, while substantiating their feasibility with economic studies considering the cost and operational difficulties in producing the nanosheets.

Several studies have proved that the incorporation of nanomaterials improves the membrane's physicochemical properties, thereby enhancing water permeation. Tremendous research needs to be carried out to verify and understand the water and ion transport in 2D-enabled TFN membranes. Studies should also evaluate the contribution of the nanopores of nanosheets in the improvement of flux. Since the introduction of TFN membranes in 2007, dedicated research work has been carried

out in this field. However, from the industrial point of view, the funds invested in the field of TFN membrane research have not successfully translated into fully functional industrial application. NanoH_2O Inc. is the only company which has launched a TFN membrane into the commercial RO membrane market.[142] Hence, further research investigations should concentrate on cost-effective technology to fabricate TFN membranes in a controllable and scalable process for industrial application.

6. Conclusions

The incorporation of 2D nanosheets offers promising prospects in manufacturing TFN membranes with enhanced performance in desalination and water purification applications. Along with the recent developments in this field, systematic review of the impact of nanosheets on membrane surface properties and performance is conducted. 2D-enabled TFN membranes are compared with commercial membranes and evaluated based on the performances in RO and NF processes for water purification. 2D nanosheets with its unique properties resulted in 2D-enabled TFN membranes with enhanced permeance, selectivity, antifouling and antibacterial performances. However, challenges in manufacturing and design of TFN membranes restricts its implementation in industrial aspects and is elaborately discussed. 2D nanosheets produced in eco-friendly, cost-effective methods, and compatible with PA layer would be the future perspectives. Advances in IP reaction techniques for membrane fabrication would be crucial in supporting 2D-enabled TFN membranes and facilitate its entry into the industrial market. 2D-enabled TFN membranes are paradigm technologies and their applications besides the water area, covered in this topic, but also in the gas and solvent separation spaces, will continue to grow over the next few years. It is also expected that besides being used for solvents, gases and water enhanced recovery, which is to date their main purpose, application in the fine chemicals, enantiomers or biomolecule separation will equally emerge.

Author contributions

Deepak Surendhra Mallya: conceptualization, visualization, writing – original draft. Ludovic F. Dumée: conceptualization, writing – review & editing, Shobha Muthukumaran: writing – review & editing, Weiwei Lei: writing – review & editing. Kanagaratnam Baskaran: writing – review & editing, supervision.

Conflicts of interest

There are no conflicts to declare.

Acknowledgements

Mr Deepak Surendhra Mallya acknowledges Deakin University for his PhD scholarship, Dr Ludovic F. Dumée acknowledges financial support from Khalifa University of Science and Technology under project RC2-2019-007, and Dr Weiwei Lei acknowledges the Australian Research Council Discovery Program (DP190103290).

References

1 Y. Ren, J. Zhu, S. Cong, J. Wang, B. Van der Bruggen, J. Liu and Y. Zhang, *J. Membr. Sci.*, 2019, **585**, 19–28.
2 Z.-M. Zhan, Z.-L. Xu, K.-K. Zhu and Y.-J. Tang, *J. Membr. Sci.*, 2020, **597**, 117640.
3 W. Lau, S. Gray, T. Matsuura, D. Emadzadeh, J. P. Chen and A. Ismail, *Water Res.*, 2015, **80**, 306–324.
4 S. P. Nunes, P. Z. Culfaz-Emecen, G. Z. Ramon, T. Visser, G. H. Koops, W. Jin and M. Ulbricht, *J. Membr. Sci.*, 2020, **598**, 117761.
5 L. He, L. F. Dumée, C. Feng, L. Velleman, R. Reis, F. She, W. Gao and L. Kong, *Desalination*, 2015, **365**, 126–135.
6 S. Lim, N. Akther, T.-H. Bae, S. Phuntsho, A. Merenda, L. F. Dumée and H. K. Shon, *Desalination*, 2020, **485**, 114461.
7 A. O. Rashed, A. Merenda, T. Kondo, M. Lima, J. Razal, L. Kong, C. Huynh and L. F. Dumée, *Sep. Purif. Technol.*, 2020, 117929.
8 L. F. Dumée, J. W. Maina, A. Merenda, R. Reis, L. He and L. Kong, *J. Membr. Sci.*, 2017, **528**, 217–224.
9 S. Abdikheibari, W. Lei, L. F. Dumée, N. Milne and K. Baskaran, *J. Mater. Chem. A*, 2018, **6**, 12066–12081.
10 Y. Rahimi-Kashkouli, M. Rahbari-Sisakht and A. Ghadami, *Environ. Sci.: Water Res. Technol.*, 2020, **6**(3), 715–723, DOI: 10.1039/c9ew00963a.
11 S. Abdikheibari, L. F. Dumée, V. Jegatheesan, Z. Mustafa, P. Le-Clech, W. Lei and K. Baskaran, *J. Water Process Eng.*, 2020, **34**, 101160.
12 S. Yang, Q. Jiang and K. Zhang, *J. Membr. Sci.*, 2020, 118052.
13 M. E. Ali, L. Wang, X. Wang and X. Feng, *Desalination*, 2016, **386**, 67–76.
14 S. Yang and K. Zhang, *J. Membr. Sci.*, 2019, 117526.
15 A. Guirguis, J. W. Maina, X. Zhang, L. C. Henderson, L. Kong, H. Shon and L. F. Dumée, *Mater. Horiz.*, 2020, **7**, 1218–1245.
16 X. Wang, Q. Li, J. Zhang, H. Huang, S. Wu and Y. Yang, *J. Membr. Sci.*, 2020, 118036.
17 M. Ge, X. Wang, S. Wu, Y. Long, Y. Yang and J. Zhang, *Sep. Purif. Technol.*, 2021, **258**, 117980.
18 L. Xu, B. Shan, C. Gao and J. Xu, *J. Membr. Sci.*, 2020, **593**, 117398.
19 H. Saleem and S. J. Zaidi, *Desalination*, 2020, **475**, 114171.
20 D. L. Zhao, S. Japip, Y. Zhang, M. Weber, C. Maletzko and T.-S. Chung, *Water Res.*, 2020, 115557.
21 M. Kumar, M. A. Khan and H. A. Arafat, *ACS Omega*, 2020, **5**(8), 3792–3800, DOI: 10.1021/acsomega.9b03975.
22 M. Bassyouni, M. Abdel-Aziz, M. S. Zoromba, S. Abdel-Hamid and E. Drioli, *J. Ind. Eng. Chem.*, 2019, **73**, 19–46.
23 M. R. Esfahani, S. A. Aktij, Z. Dabaghian, M. D. Firouzjaei, A. Rahimpour, J. Eke, I. C. Escobar, M. Abolhassani, L. F. Greenlee and A. R. Esfahani, *Sep. Purif. Technol.*, 2018, **213**, 465–499.

24 B. Al-Najar, C. D. Peters, H. Albuflasa and N. P. Hankins, *Desalination*, 2020, **479**, 114323.
25 S. Kim, H. Wang and Y. M. Lee, *Angew. Chem.*, 2019, **131**, 17674–17689.
26 Y. Su, D. Liu, G. Yang, Q. Han, Y. Qian, Y. Liu, L. Wang, J. M. Razal and W. Lei, *ACS Appl. Mater. Interfaces*, 2020, **12**, 45453–45459.
27 F. Moghadam and H. B. Park, *2D Mater.*, 2019, **6**, 042002.
28 Y. Cheng, Y. Pu and D. Zhao, *Chem. – Asian J.*, 2020, **15**(15), 2241–2270.
29 Z. Liao, J. Zhu, X. Li and B. Van der Bruggen, *Sep. Purif. Technol.*, 2021, **266**, 118567.
30 J. Yang, Z. Li, Z. Wang, S. Yuan, Y. Li, W. Zhao and X. Zhang, *Adv. Mater. Technol.*, 2021, 2000862.
31 P. Zhao, J. Wang, X. Han, J. Liu, Y. Zhang and B. Van der Bruggen, *Ind. Eng. Chem. Res.*, 2021, **60**(4), 1850–1858.
32 D.-D. Shao, W.-J. Yang, H.-F. Xiao, Z.-Y. Wang, C. Zhou, X.-L. Cao and S.-P. Sun, *ACS Appl. Mater. Interfaces*, 2019, **12**, 580–590.
33 S. Yu, S. Li, S. Huang, Z. Zeng, S. Cui and Y. Liu, *J. Membr. Sci.*, 2017, **540**, 155–164.
34 P. Kumari, N. Bahadur and L. F. Dumée, *Sep. Purif. Technol.*, 2020, **230**, 115878.
35 R. Al-Attabi, J. Rodriguez-Andres, J. A. Schütz, M. Bechelany, E. Des Ligneris, X. Chen, L. Kong, Y. S. Morsi and L. F. Dumée, *Sep. Purif. Technol.*, 2019, **229**, 115806.
36 J. Nambikkattu, N. J. Kaleekkal and J. P. Jacob, *Environ. Sci. Pollut. Res.*, 2020, 1–13.
37 H. Zhang, Y. Wang, Y. Wei, C. Gao and G. Zhu, *J. Appl. Polym. Sci.*, 2020, 49030.
38 L. Ren, J. Chen, Q. Lu, C. Wang, J. Han, K. Huang, X. Pan and H. Wu, *J. Membr. Sci.*, 2020, **597**, 117641.
39 M. Q. Seah, W. J. Lau, P. S. Goh, H.-H. Tseng, R. A. Wahab and A. F. Ismail, *Polymers*, 2020, **12**, 2817.
40 B.-Q. Huang, Y.-J. Tang, Z.-X. Zeng and Z.-L. Xu, *J. Membr. Sci.*, 2020, **596**, 117718.
41 Z.-M. Zhan, Z.-L. Xu, K.-K. Zhu, S.-M. Xue, C.-H. Ji, B.-Q. Huang, C. Y. Tang and Y.-J. Tang, *J. Membr. Sci.*, 2020, 118067.
42 Q. Xie, S. Zhang, Z. Xiao, X. Hu, Z. Hong, R. Yi, W. Shao and Q. Wang, *RSC Adv.*, 2017, **7**, 18755–18764.
43 Y. Wen, X. Zhang, X. Li, Z. Wang and C. Y. Tang, *ACS Appl. Nano Mater.*, 2020, **3**, 9238–9248.
44 Z. Yang, P.-F. Sun, X. Li, B. Gan, L. Wang, X. Song, H.-D. Park and C. Y. Tang, *Environ. Sci. Technol.*, 2020, **54**(24), 15563–15583.
45 S. Abdikheibari, W. Lei, L. F. Dumée, A. J. Barlow and K. Baskaran, *Appl. Surf. Sci.*, 2019, **488**, 565–577.
46 A. Inurria, P. Cay-Durgun, D. Rice, H. Zhang, D.-K. Seo, M. L. Lind and F. Perreault, *Desalination*, 2019, **451**, 139–147.
47 J. R. Werber, C. O. Osuji and M. Elimelech, *Nat. Rev. Mater.*, 2016, **1**, 1–15.
48 S. Bano, A. Mahmood, S.-J. Kim and K.-H. Lee, *J. Mater. Chem. A*, 2015, **3**, 2065–2071.
49 H.-R. Chae, J. Lee, C.-H. Lee, I.-C. Kim and P.-K. Park, *J. Membr. Sci.*, 2015, **483**, 128–135.
50 S. Xia, L. Yao, Y. Zhao, N. Li and Y. Zheng, *Chem. Eng. J.*, 2015, **280**, 720–727.
51 Y. Kang, M. Obaid, J. Jang and I. S. Kim, *Desalination*, 2019, **470**, 114125.
52 J. Yin, G. Zhu and B. Deng, *Desalination*, 2016, **379**, 93–101.
53 H. L. Poh, F. Šaněk, A. Ambrosi, G. Zhao, Z. Sofer and M. Pumera, *Nanoscale*, 2012, **4**, 3515–3522.
54 Y. Zhang, H. Ruan, C. Guo, J. Liao, J. Shen and C. Gao, *Sep. Purif. Technol.*, 2020, **234**, 116017.
55 B. Pant, P. Pokharel, A. P. Tiwari, P. S. Saud, M. Park, Z. K. Ghouri, S. Choi, S.-J. Park and H.-Y. Kim, *Ceram. Int.*, 2015, **41**, 5656–5662.
56 J. Li, G. Wang, H. Zhu, M. Zhang, X. Zheng, Z. Di, X. Liu and X. Wang, *Sci. Rep.*, 2014, **4**, 1–8.
57 H. Abadikhah, E. Naderi Kalali, S. Khodi, X. Xu and S. Agathopoulos, *ACS Appl. Mater. Interfaces*, 2019, **11**(26), 23535–23545.
58 F. A. A. Ali, J. Alam, A. K. Shukla, M. Alhoshan, J. M. Khaled, W. A. Al-Masry, N. S. Alharbi and M. Alam, *J. Ind. Eng. Chem.*, 2019, **80**, 227–238.
59 A. F. Faria, C. Liu, M. Xie, F. Perreault, L. D. Nghiem, J. Ma and M. Elimelech, *J. Membr. Sci.*, 2017, **525**, 146–156.
60 J. Zhu, J. Wang, A. A. Uliana, M. Tian, Y. Zhang, Y. Zhang, A. Volodin, K. Simoens, S. Yuan and J. Li, *ACS Appl. Mater. Interfaces*, 2017, **9**, 28990–29001.
61 H. Abadikhah, E. N. Kalali, S. Behzadi, S. A. Khan, X. Xu, M. E. Shabestari and S. Agathopoulos, *Chem. Eng. Sci.*, 2019, **204**, 99–109.
62 R. Rajakumaran, V. Boddu, M. Kumar, M. S. Shalaby, H. Abdallah and R. Chetty, *Desalination*, 2019, **467**, 245–256.
63 N. Izadmehr, Y. Mansourpanah, M. Ulbricht, A. Rahimpour and M. R. Omidkhah, *J. Environ. Manage.*, 2020, **276**, 111299.
64 W. Shao, C. Liu, H. Ma, Z. Hong, Q. Xie and Y. Lu, *Appl. Surf. Sci.*, 2019, **487**, 1209–1221.
65 Q. Xie, W. Shao, S. Zhang, Z. Hong, Q. Wang and B. Zeng, *RSC Adv.*, 2017, **7**, 54898–54910.
66 Q. Xie, S. Zhang, Z. Hong, H. Ma, B. Zeng, X. Gong, W. Shao and Q. Wang, *Chem. Eng. J.*, 2019, **368**, 186–201.
67 J. Chen, Z. Li, C. Wang, H. Wu and G. Liu, *RSC Adv.*, 2016, **6**, 112148–112157.
68 S. S. Shahabi, N. Azizi and V. Vatanpour, *Sep. Purif. Technol.*, 2019, **215**, 430–440.
69 X. Gao, Y. Li, X. Yang, Y. Shang, Y. Wang, B. Gao and Z. Wang, *J. Mater. Chem. A*, 2017, **5**, 19875–19883.
70 S. S. Shahabi, N. Azizi, V. Vatanpour and N. Yousefimehr, *Sep. Purif. Technol.*, 2020, **235**, 116134.
71 Q. Bi, C. Zhang, J. Liu, Q. Cheng and S. Xu, *Water Sci. Technol.*, 2020, **81**, 253–264.
72 Y. Liu, X. Wang, X. Gao, J. Zheng, J. Wang, A. Volodin, Y. F. Xie, X. Huang, B. Van der Bruggen and J. Zhu, *J. Membr. Sci.*, 2020, **596**, 117717.
73 D. Golberg, Y. Bando, Y. Huang, T. Terao, M. Mitome, C. Tang and C. Zhi, *ACS Nano*, 2010, **4**, 2979–2993.
74 W. Lei, V. N. Mochalin, D. Liu, S. Qin, Y. Gogotsi and Y. Chen, *Nat. Commun.*, 2015, **6**, 8849.

75 C. Chen, S. Qin, D. Liu, J. Wang, G. Yang, Y. Su, L. Zhang, W. Cao, M. Ma and Y. Qian, *ACS Appl. Mater. Interfaces*, 2019, **11**, 30430–30436.
76 R. Wang, Z.-X. Low, S. Liu, Y. Wang, S. Murthy, W. Shen and H. Wang, *J. Membr. Sci.*, 2020, 118389.
77 T. Hyun, J. Jeong, A. Chae, Y. K. Kim and D.-Y. Koh, *BMC Chem. Eng.*, 2019, **1**, 12.
78 Y. Li, S. Yang, K. Zhang and B. Van der Bruggen, *Desalination*, 2019, **454**, 48–58.
79 W. Hu, X. Cui, L. Xiang, L. Gong, L. Zhang, M. Gao, W. Wang, J. Zhang, F. Liu and B. Yan, *J. Colloid Interface Sci.*, 2020, **560**, 177–185.
80 Z. Wang, Q. Tu, S. Zheng, J. J. Urban, S. Li and B. Mi, *Nano Lett.*, 2017, **17**, 7289–7298.
81 G. Guan, M. You, X. Liu, Y. L. Wu, E. Ye and Z. Li, *Adv. Mater. Interfaces*, 2019, **6**, 1900585.
82 Z. Mohammadpour, S. H. Abdollahi and A. Safavi, *ACS Appl. Energy Mater.*, 2018, **1**, 5896–5906.
83 C. Zhang, D.-F. Hu, J.-W. Xu, M.-Q. Ma, H. Xing, K. Yao, J. Ji and Z.-K. Xu, *ACS Nano*, 2018, **12**, 12347–12356.
84 M.-Q. Ma, C. Zhang, C.-Y. Zhu, S. Huang, J. Yang and Z.-K. Xu, *J. Membr. Sci.*, 2019, **591**, 117316.
85 H. Zhang, X.-Y. Gong, W.-X. Li, X.-H. Ma, C. Y. Tang and Z.-L. Xu, *J. Membr. Sci.*, 2020, 118605.
86 L. Ding, Y. Wei, Y. Wang, H. Chen, J. Caro and H. Wang, *Angew. Chem., Int. Ed.*, 2017, **56**, 1825–1829.
87 I. Ihsanullah, *Nano-Micro Lett.*, 2020, **12**, 1–20.
88 T. Liu, X. Liu, N. Graham, W. Yu and K. Sun, *J. Membr. Sci.*, 2020, **593**, 117431.
89 I. Ihsanullah, *Chem. Eng. J.*, 2020, 124340.
90 K. Rasool, R. P. Pandey, P. A. Rasheed, S. Buczek, Y. Gogotsi and K. A. Mahmoud, *Mater. Today*, 2019, **30**, 80–102.
91 Y. A. Al-Hamadani, B.-M. Jun, M. Yoon, N. Taheri-Qazvini, S. A. Snyder, M. Jang, J. Heo and Y. Yoon, *Chemosphere*, 2020, 126821.
92 G. Yang, W. Lei, C. Chen, S. Qin, L. Zhang, Y. Su, J. Wang, Z. Chen, L. Sun and X. Wang, *Nano Energy*, 2020, **75**, 104954.
93 Y. Z. Tan, H. Wang, L. Han, M. B. Tanis-Kanbur, M. V. Pranav and J. W. Chew, *J. Membr. Sci.*, 2018, **565**, 254–265.
94 R. Han and P. Wu, *J. Mater. Chem. A*, 2019, **7**, 6475–6481.
95 S. Wei, Y. Xie, Y. Xing, L. Wang, H. Ye, X. Xiong, S. Wang and K. Han, *J. Membr. Sci.*, 2019, **582**, 414–422.
96 K. Rasool, K. A. Mahmoud, D. J. Johnson, M. Helal, G. R. Berdiyorov and Y. Gogotsi, *Sci. Rep.*, 2017, **7**, 1–11.
97 R. P. Pandey, K. Rasool, V. E. Madhavan, B. Aïssa, Y. Gogotsi and K. A. Mahmoud, *J. Mater. Chem. A*, 2018, **6**, 3522–3533.
98 Z. Xia, Y. Zhao and S. B. Darling, *Adv. Mater. Interfaces*, 2020, 2001507.
99 S. Yuan, X. Li, J. Zhu, G. Zhang, P. Van Puyvelde and B. Van der Bruggen, *Chem. Soc. Rev.*, 2019, **48**, 2665–2681.
100 Z. Zhang, C. Yin, G. Yang, A. Xiao, X. Shi, W. Xing and Y. Wang, *J. Membr. Sci.*, 2021, **618**, 118754.
101 L.-L. Liu, J. Chen, Y. Zhang, C.-X. Yu, W. Du, X.-Q. Sun, J.-L. Zhang, F.-L. Hu, Y. Mi and L.-F. Ma, *J. Mater. Chem. A*, 2021, **9**, 546–555.
102 Z. W. Jiang, T. T. Zhao, S. J. Zhen, C. M. Li, Y. F. Li and C. Z. Huang, *J. Mater. Chem. A*, 2021, **9**, 9301–9306.
103 S. Yadav, R. Dixit, S. Sharma, S. Dutta, K. Solanki and R. K. Sharma, *Mater. Adv.*, 2021, **2**(7), 2153–2187, DOI: 10.1039/D0MA00982B.
104 M. Varsha and G. Nageswaran, *J. Electrochem. Soc.*, 2020, **167**, 136502.
105 J. Jin, Y.-f. Zhang, H. Wang, Y. Gong, R. Wang, B. He, T. Xiao, Y. Zheng, X. Liu and K. Zhou, *Mater. Chem. Front.*, 2021, DOI: 10.1039/d0qm01011a.
106 S. Li, J. Lin, W. Xiong, X. Guo, D. Wu, Q. Zhang, Q.-L. Zhu and L. Zhang, *Coord. Chem. Rev.*, 2021, **438**, 213872.
107 B.-M. Jun, Y. A. Al-Hamadani, A. Son, C. M. Park, M. Jang, A. Jang, N. C. Kim and Y. Yoon, *Sep. Purif. Technol.*, 2020, 116947.
108 Q. Zhao, D. L. Zhao and T.-S. Chung, *J. Membr. Sci.*, 2021, **625**, 119158.
109 B. Zhao, X. Long, H. Wang, L. Wang, Y. Qian, H. Zhang, C. Yang, Z. Zhang, J. Li and C. Ma, *Colloids Surf., A*, 2021, **612**, 125971.
110 D. L. Zhao, W. S. Yeung, Q. Zhao and T.-S. Chung, *J. Membr. Sci.*, 2020, 118039.
111 G. Gnanasekaran, S. Balaguru, G. Arthanareeswaran and D. B. Das, *Sep. Sci. Technol.*, 2019, **54**, 434–446.
112 R. Dai, X. Wang, C. Y. Tang and Z. Wang, *Environ. Sci. Technol.*, 2020, **54**, 7619–7628.
113 R. Dai, X. Zhang, M. Liu, Z. Wu and Z. Wang, *J. Membr. Sci.*, 2019, **573**, 46–54.
114 Y.-y. Zhao, Y.-l. Liu, X.-m. Wang, X. Huang and Y. F. Xie, *ACS Appl. Mater. Interfaces*, 2019, **11**, 13724–13734.
115 M. Zhang, W. Jin, F. Yang, M. Duke, Y. Dong and C. Y. Tang, *Environ. Sci. Technol.*, 2020, **54**, 7715–7724.
116 L. Wang, M. Fang, J. Liu, J. He, L. Deng, J. Li and J. Lei, *RSC Adv.*, 2015, **5**, 50942–50954.
117 D. G. Papageorgiou, I. A. Kinloch and R. J. Young, *Prog. Mater. Sci.*, 2017, **90**, 75–127.
118 J. Kucera, *Membranes*, 2019, **9**, 111.
119 M. Y. Ashfaq, M. A. Al-Ghouti and N. Zouari, *Carbon*, 2020, **166**, 374–387.
120 N. Li, L. Yu, Z. Xiao, C. Jiang, B. Gao and Z. Wang, *Desalination*, 2020, **473**, 114162.
121 Z. Yang, X.-H. Ma and C. Y. Tang, *Desalination*, 2018, **434**, 37–59.
122 Y. Okamoto and J. H. Lienhard, *Desalination*, 2019, **470**, 114064.
123 A. Karabelas, C. Koutsou, M. Kostoglou and D. Sioutopoulos, *Desalination*, 2018, **431**, 15–21.
124 M. C. Garg and H. Joshi, *Water Sci. Technol.: Water Supply*, 2015, **15**, 1027–1033.
125 A. Zhu, A. Rahardianto, P. D. Christofides and Y. Cohen, *Desalin. Water Treat.*, 2010, **15**, 256–266.
126 K. Divya, M. S. S. A. Saraswathi, S. Alwarappan, A. Nagendran and D. Rana, *Polymer*, 2018, **155**, 42–49.
127 P. Cheng, Y. Chen, X. Yan, Y. Wang and W. Z. Lang, *ChemSusChem*, 2019, **12**, 275–282.
128 L. Shen, W.-s. Hung, J. Zuo, X. Zhang, J.-Y. Lai and Y. Wang, *J. Membr. Sci.*, 2019, **570**, 112–119.

129 L. Shen, W.-s. Hung, J. Zuo, L. Tian, M. Yi, C. Ding and Y. Wang, *J. Membr. Sci.*, 2020, 117834.
130 X. Kang, X. Liu, J. Liu, Y. Wen, J. Qi and X. Li, *Appl. Surf. Sci.*, 2020, **508**, 145198.
131 J. B. Morales-Cuevas, S. Pérez-Sicairos, S. W. Lin and M. I. Salazar-Gastélum, *J. Appl. Polym. Sci.*, 2019, **136**, 48129.
132 C. Jiang, L. Zhang, P. Li, H. Sun, Y. Hou and Q. J. Niu, *ACS Appl. Mater. Interfaces*, 2020, **12**, 25304–25315.
133 J. Chen, J. Zhang, X. Wu, X. Cui, W. Li, H. Zhang, J. Wang, X.-Z. Cao and P. Zhang, *J. Mater. Chem. A*, 2020, **8**, 9160–9167.
134 N. A. Khan, J. Yuan, H. Wu, T. Huang, X. You, M. A. Olson, C. S. Azad, A. U. Rahman and Z. Jiang, *ACS Appl. Mater. Interfaces*, 2020, **12**(24), 27777–27785.
135 X. Wang, T.-M. Yeh, Z. Wang, R. Yang, R. Wang, H. Ma, B. S. Hsiao and B. Chu, *Polymer*, 2014, **55**, 1358–1366.
136 K. Shen, C. Cheng, T. Zhang and X. Wang, *J. Membr. Sci.*, 2019, **588**, 117192.
137 Sigma-Aldrich, Graphene Oxide Products, https://www.sigmaaldrich.com/catalog/product/aldrich/763713?lang=en&region=US (accessed March 1, 2021).
138 Sigma-Aldrich, Boron Nitride Nanoplatelet Products, https://www.sigmaaldrich.com/catalog/product/aldrich/900405?lang=en&region=US, (accessed March 01 2021, 2021).
139 Sigma-Aldrich, Molybdenum Disulfide Nanoplatelets Products, https://www.sigmaaldrich.com/catalog/product/aldrich/901792?lang=en&region=US, (accessed March 01 2021, 2021).
140 S.-H. Park, A. Alammar, Z. Fulop, B. A. Pulido, S. P. Nunes and G. Szekely, *Green Chem.*, 2021, **23**(3), 1175–1184, DOI: 10.1039/d0gc03226c.
141 L. Shen, Q. Xie, Z. Hong, C. Wu, T. Yu, H. Fang, Y. Xiong, G. Zhang, Y. Lu and W. Shao, *Ind. Eng. Chem. Res.*, 2020, **59**, 19001–19011.
142 D. S. Dlamini, B. B. Mamba and J. Li, *Sci. Total Environ.*, 2019, **656**, 723–731.
143 L. Peng, Z. Xu, Z. Liu, Y. Wei, H. Sun, Z. Li, X. Zhao and C. Gao, *Nat. Commun.*, 2015, **6**, 1–9.
144 L. Ding, Y. Wei, L. Li, T. Zhang, H. Wang, J. Xue, L.-X. Ding, S. Wang, J. Caro and Y. Gogotsi, *Nat. Commun.*, 2018, **9**, 1–7.
145 S. Wan, J. Guo, J. Kim, H. Ihee and D. Jiang, *Angew. Chem., Int. Ed.*, 2008, **47**, 8826–8830.